

## Durability of UHPFRC functionalised with nanoadditives due to synergies in the action of sulphate and chloride in cracked and uncracked states

✉ M. Giménez, M.C. Alonso, E. Menéndez, M. Criado

Instituto de Ciencias de la Construcción Eduardo Torroja (IETcc-CSIC) (Madrid, Spain)  
✉: mercedes.gimenez@ietcc.csic.es

Received 15 September 2021

Accepted 8 November 2021

Available on line 1 December 2021

**ABSTRACT:** This paper studies the durability of Ultra High Performance Fibre Reinforced Concrete (UHPFRC) with high Blast Furnace Slag content (BFS) and nanoadditives such as crystalline admixture (CA), alumina nanofibres (ANF) and cellulose nanocrystals (CNC), exposed to different aggressive environmental conditions: 1) three aggressive media: a) deionized water (dw), b) sulphate rich solution (ss) and c) simulated geothermal water (sgw) containing sulphate and chloride; 2) two water interaction conditions: a) static and b) dynamic (water impact); and 3) with and without the presence of cracks. Durability was analysed over 24 months, measuring several physical and chemical parameters of the system, recording changes in both the aggressive media and the concrete. All UHPFRC types demonstrate good durability, showing high resistance to expansion and deformation in the sulphate-rich media. A leaching process occurs in all water interaction systems, the dynamic interaction in sgw being the most aggressive. The interaction of sgw inside the crack favours the formation of solid phases such as calcium carbonates and ettringite, while the presence of nanoadditives affects the response of both the matrix and the formation of precipitates within the crack.

**KEY WORDS:** HPC; Nanoadditives; Sulphate; Chloride; Cracking.

**Citation/Citar como:** Giménez, M.; Alonso, M.C.; Menéndez, E.; Criado, M. (2021) Durability of UHPFRC functionalised with nanoadditives due to synergies in the action of sulphate and chloride in cracked and uncracked states. Mater. Construcc. 71 [344], e264. <https://doi.org/10.3989/mc.2021.14021>.

**RESUMEN:** *Durabilidad de UHPFRC funcionalizados con nanoaditivos por la acción sinérgica de sulfatos y cloruros en estado fisurado y no fisurado.* El objetivo de este trabajo está enfocado en el estudio de la durabilidad de hormigones de ultra altas prestaciones reforzados con fibras (UHPFRC) con alto contenido en escoria de alto horno (BSF) y nanoaditivos como aditivo cristalino (CA), nanofibras de alúmina (ANF) y nanocristales de celulosa (CNC), expuestos a diferentes condiciones ambientales agresivas: 1) Tres medios agresivos: a) agua desionizada (dw), b) rico en sulfatos (ss) y c) agua geotérmica simulada (sgw) que contiene sulfatos y cloruros; 2) dos condiciones de interacción de agua: a) estática y b) dinámica (impacto de agua); y 3) con y sin la presencia de fisuras. La durabilidad fue analizada durante 24 meses, midiendo varios parámetros físico-químicos del sistema, informando acerca de los cambios en el medio agresivo y en el hormigón. Todos los tipos de UHPFRC demostraron buena durabilidad mostrando una alta resistencia a la expansión y a la deformación en medios de alto contenido en sulfatos. Un proceso de lixiviación tuvo lugar en todos los sistemas de interacción, siendo el dinámico en sgw el más agresivo. La interacción del sgw dentro de la fisura favorece la formación de fases sólidas como carbonatos de calcio y etringita, mientras que la presencia de nanoaditivos afecta a la respuesta de la matriz, así como la formación de precipitados dentro de la fisura.

**PALABRAS CLAVE:** UHPFRC; Nanoaditivos; Sulfatos; Cloruros; Fisuración.

**Copyright:** ©2021 CSIC. This is an open-access article distributed under the terms of the Creative Commons Attribution 4.0 International (CC BY 4.0) License.

## 1. INTRODUCTION

The use of concrete in structures is generalised around the world (1). The traditional material, known as conventional concrete (CC), has been improved continuously through the optimal use and dosage of its components (cement, water, mineral additions, fibres or additives) in order to enhance its performance, and upgraded as Ultra High Performance Concretes (UHPC) (2, 3). In this sense, ultra-high-performance fibre-reinforced concretes (UHPFRC) satisfy the demands of today's construction by including different types of fibres (4). Steel fibre reinforcement is included to improve tensile strength behaviour by reducing brittle failure (5, 6). As UHPC, the high density and low permeability due to the reduced water to binder ratio (lower than 0.2) and a maximum aggregate diameter of less than 1–2 mm give rise to high compression strength concretes (150–200 MPa) with high density. The inclusion of steel fibres leads to high ductility in tension and bending, with tensile strength values higher than 7 MPa. Due to these superior mechanical properties and its high-toughness performance (3), UHPFRC has become an attractive alternative concrete for the construction of high-elevation buildings, pre-stressed girders or long-span bridges.

UHPFRCs meet not only the structural requirements but also the durability requirements that must be met for proper response of the material. There have been different approaches in recent years to upgrade durability (5-9). One of the actions to extend the durability of concretes against some aggressive environments has been the inclusion of mineral additions such as blast furnace slag (BFS) or fly ash (9), which modify the pore structure and increase the chloride binding capacity (10) and improve resistance to sulphate attack (11-13).

The type of environment plays an important role in the durability response of concrete structures. Some of the main risks that are common environmental causes of a loss of durability are related to rebar corrosion or concrete damage due to freeze and thaw, sulphate chemical attack, leaching or erosion. Aggressive scenarios can present single or combined hazards, with many kinds and concentrations of aggressive ions, but characteristics such as temperature and moisture content can affect durability. These two parameters could accelerate ion transport and interaction, leading to the destruction of concrete components and their integrity and thus reducing the service life of concrete structures (14).

Several studies (14-16) have been carried out to address the durability of UHPFRC in aggressive environments and the effects of temperature and moisture. Oh *et al.* (15) reported that increases in temperature and relative humidity greatly increased chloride penetration in concretes. Yin *et al.* (16) observed that the mechanical interfacial bending

strength between fibre and concrete decreased with increases in chloride in dry-wet and freeze-thaw cycles. Song *et al.* (14) studied the variation in macro/micro characteristics of UHPFRCs under attack in critical marine environments, such as high-temperature seawater, dry-wet cycle seawater and normal seawater. The high temperature accelerated the diffusion rate of ions and the dry-wet cycle caused differences in ion concentrations between the surface and the inner part of the concretes; both significantly accelerated attack by Cl ions. They also observed that temperature exerted a significant influence and led to the most serious deterioration of UHPFRC. The interaction of UHPFRC with low ionic waters was studied by Alonso *et al.* (17) using different interaction regimes, in a tank and in running water, which affected the leaching processes and the contribution of the high content of anhydrous cement in these concretes. Therefore, environmental conditions exert a great influence on the durability of UHPFRC, although many uncertainties remain. This article considers the effect of new elements within the interaction between environmental conditions and UHPFRC: the joint action of water impact and ion aggressiveness. The impact of water on the concrete surface can produce several concurrent deterioration actions: erosion of the surface, leaching of cement paste and aggressive ions interacting and forming phases with different physical and chemical stability. These types of deteriorations have been found in the basins of cooling-water towers from a geothermal power plant (H2020 ReSHEALience GA760824), where the extracted water (rich in sulphate and chloride) falls from a height of 10 m from the cooling water tower to a basin made of conventional concrete.

The risks caused by aggressive environments in the specific case of UHPFRCs are related to fibre performance and concrete integrity. The fibre response against environmental actions will depend on the composition of the fibres. In the case of steel fibres, the main risk will be corrosion (18). The dense system of UHPFRCs is disturbed and deteriorated by the addition of a great amount of steel fibre, which is a conductor to the entry of ions; and this high steel fibre content causes corrosion as well (14, 19). Conversely, the concrete bulk could be affected by the action of aggressive substances such as chloride, sulphates, or magnesium ions in seawater, which can cause synergy actions and complex reactions with the concrete. The ion content of the aggressive waters interacting with concretes has a significant influence, as was observed by García-Calvo *et al.* (20), specifically in the penetration of Cl in the cement matrix and calcium silicate hydrate (C-S-H) gel alteration. Chloride ions can penetrate the cementitious concrete matrix exposed to chloride salt solutions via diffusion and absorption processes (21). Some free chloride ions are left in the pore solution,

while the cement matrix binds a certain proportion of chloride ions which can be trapped by the C-S-H gel and react with calcium aluminate ( $C_3A$ ) phases and monosulphoaluminate (AFm) to form Friedel's salt ( $Ca_4Al_2(OH)_{12}Cl_2 \cdot 4H_2O$ ) (21, 22), thus modifying the microstructure. The external sulphate ions ( $SO_4^{2-}$ ) also enter the porous cement and interact with the cement hydration products; portlandite  $Ca(OH)_2$  can interact with sulphate ions and become gypsum ( $CaSO_4 \cdot 2H_2O$ ), and the combination of monosulphate ( $3CaO \cdot Al_2O_3 \cdot CaSO_4 \cdot 12H_2O$ ) and external sulphate forms ettringite ( $3CaO \cdot Al_2O_3 \cdot 3CaSO_4 \cdot 32H_2O$ ) (21, 23). Both products (gypsum and ettringite) occupy a greater volume after crystallization in the concrete pores than the compounds they replace, leading to expansion, cracking, and ultimately the transformation of the material into a non-cohesive material (21, 24-26).

While significant studies have been performed with each single ion,  $Cl^-$  or  $SO_4^{2-}$ , there is scarce information on the coexistence of both ions in the aggressive environment. In addition to that, in real scenarios, structures are subjected to the simultaneous action of exposure agents as defined by the exposure classes, and therefore the synergy and interaction between different aggressive causes including different physical and chemical sources should be assessed, although construction codes do not consider the combination of actions.

De Weerd et al. (23) observed a reduction in chloride binding due to the presence of additional sulphate, attributed to the preferential reaction of the latter with phases containing aluminate, reducing the formation of Friedel's salt. In agreement with this finding, some studies on conventional concrete by Alonso et al. (25) have demonstrated that both ions penetrate and interact with the cement matrix, but sulphates induce the formation of new phases such as ettringite and free chloride continues penetrating deeper and faster into the matrix. However, Cheng et al. (22) reported the contrary, that sulphate ions enhance the chemical absorption of chloride ions, promoting the formation of Friedel's salt, reducing the pore size and closing the channels for  $Cl^-$  ion penetration (26). These controversies highlight the need to carry out more studies on the influence of the joint interaction of these two aggressive agents on concrete structures and specifically on UHPFRCs, for which there is still a great lack of information on their durability under these conditions.

On the other hand, concrete structures are designed to operate in a cracked state. Cracks may influence the durability response of the material by weakening it, as they create paths for the aggressive substances to enter into the concrete bulk, reducing its service life (18, 27, 28). Again, durability studies in cracked concrete related to chemical interactions with the aggressive environment are scarce and less common in the case of UHPFRC.

A well-known method for reducing cracking is the inclusion of fibres (18, 29). But the inclusion of additives also enhances the behaviour of concrete against cracks (30-33). Overall, the nano and micro size of the additives used result in a refinement of the microstructure by densifying the pore structure (33-37), the inclusion of small particles acting as a filler and, in addition, giving rise to more nucleation points due to their high surface area to volume ratio, which stimulates cement hydration (33-35, 37).

One of these additives is crystalline admixtures (38), which act as a pore-blocking precipitate when reacting with cement and water, giving rise to a denser pore structure and the sealing of cracks (39-42). Alumina nanofibres can modify the pore structure. Some authors have found that nanofibers can accelerate the cement hydration process and lead to a denser and more compact concrete matrix by creating larger volumes of reaction products; alumina nanofibers also control crack initiation and growth (35, 37, 39). This is also supported by Behfarnia et al. (43), where the frost resistance of concrete containing alumina nanofibres was considerably improved, with compaction of its microstructure, and showed better behaviour than concrete containing the same amount of nano- $SiO_2$ . On the other hand, the reduction of cracks due to shrinkage is controlled by the inclusion of cellulose nanocrystals, which also densify the interfacial transition zone (44-46). The addition of 2% cellulose fibres by weight of cement was found to reduce by 32% the autogenous shrinkage of cement paste at 7 days due to the internal curing water that cellulose fibres are able to provide to the hydrating paste (45, 47). Cellulose nanofibres can reduce and delay crack propagation as well as prompt hydration (46, 48).

This paper assesses the combined action of physical (dynamic/static) and chemical actions in UHPFRC, leading to four main scenarios. The chemical influence of the environment considering: interaction of water with no inclusion of aggressive ions (deionised water), isolated sulphate action in standardised conditions, and joint action of sulphate and chloride in simulated geothermal water systems, which consist of a laboratory duplicate of the water used in the cooling processes of geothermal plants. The sulphate solution was tested at  $5^\circ C$  in order to promote the aggressiveness of the solution, while the simulated geothermal water was tested at  $20 \pm 2^\circ C$ , similar to the simulated exposure conditions. The physical action in the dynamic test (water impact) simulates the real scenario of the cooling tower in the geothermal power plant, in which the relevant physical damage due to the impact of water was the erosion phenomenon taking place in conventional concrete.

The influence of the nanoadditives, the uncracked or cracked state and the physical and chemical environmental conditions is evaluated by the separate

and joint analysis of the selected parameters in order to study not only the single effect of the aggressive ions and conditions, but also the synergy between the aggressive substances and actions of each scenario.

## 2. MATERIALS AND METHODS

### 2.1 Materials

High-performance fibre-reinforced concretes (HPFRCs) including BFS and various types of nanoadditives have been designed by Politecnico di Milano (46) as part of the H2020 ReSHEALience project (GA760824). The additives used to modify the concrete characteristics are crystalline admixture (CA) (38), alumina nanofibers (ANF) and cellulose nanocrystals (CNC). The dosage of the mixes including slag (45%) and the nanoadditives are the same described in (46), with a water to binder ratio of 0.18. The percentages of nanoadditives selected for the mixes are summarised in Table 1. The porosity of the studied concretes was measured by mercury intrusion porosimetry. The inclusion of nanoadditives such as ANF and CNC contributed to reducing the total porosity (XA-CA 4.5%, XA-CA+ANF 3% and XA-CA+CNC 4%), as detailed in (47).

TABLE 1. Percentages of nanoadditives per concrete mix (46).

Constituents [kg/m <sup>3</sup> ]	XA-CA	XA-CA+ANF	XA-CA+CNC
CEM I 52.5 R		600	
Slag		500	
Water		200	
Steel fibres Azichem Ready-mesh 200		120	
Sand 0-2 mm		982	
Superplasticizer Glenium ACE 300		33	
Crystalline admixtures		4.8	
Alumina nanofibers [% by weight of cement]	0	0.25	0
Cellulose nanocrystals [% by weight of cement]	0	0	0.15

The concretes were cast in Ø100x300 mm cylinders and 40x40x160 mm prisms and cured in a moist room at 20 °C and 95% RH for at least two months. Six samples of Ø100x50 mm per type of concrete were obtained from the original cylinders for leaching and erosion studies. For each type of concrete, 3 samples were left uncracked, while 5 mm notches were performed on the other 3 (Figure 1), which were cracked according to the procedure described below. The prism samples had two studs incorporated at both sides of 40x40 mm faces to determine dimensional changes, with ten samples per type of concrete.

### 2.2. Methods

#### 2.2.1 Aggressive media

Three environments were selected regarding water aggressiveness: 1) no inclusion of chemically aggressive ions – deionised water (dw); 2) aggressive sulphate rich solution (ss) according to ASTM C1012-04; and 3) water contaminated with sulphate and chloride simulating the cooling water of a geothermal plant (sgw) (47). Table 2 includes the chemical composition of the aggressive waters, the temperatures used in the study and the pH. In the case of sgw, the pH was adjusted to 3 with HNO<sub>3</sub>.

#### 2.2.2 Types of aggressive interaction

In order to study the interaction of the UHPFRC including nanoadditives with a multi-ion aggressive environment that includes sulphates plus chlorides, two types of water interaction conditions were established: dynamic and static. The dynamic interaction was performed using two of the aggressive media: deionised water (dw) and simulated geothermal water (sgw) at laboratory temperature (20 ± 2 °C). The static tests were performed using simulated geothermal water at 20 ± 2 °C and the sulphate rich solution (ss) at 5 °C (Table 2).

*The dynamic test arrangement* (Figure 1 - left) was specifically designed to study the physical impact of water. The test arrangement consisted of a plastic container in which a specimen was placed over a plastic mesh to avoid immersion in the aggressive media. A pump was joined to a rubber tube allowing recirculation of the water and the impact of

Table 2 Simulated geothermal water and sulphate solution compositions (in ppm).

Aggressive agent	Type of aggressive media	T (°C)	pH	SO <sub>4</sub> <sup>2-</sup>	Cl <sup>-</sup>	Ca <sup>2+</sup>	K <sup>+</sup>	Na <sup>+</sup>
No ion	Deionized water (dw)	20±2	6.5	-	-	-	-	-
Sulphate	Sulphate solution from ASTM C1012-04 (ss)	5	6.8	6760	-	-	-	3240
Sulphate+Cl	Simulated geothermal water (sgw)	20±2	3	2300	300	4	20	1280

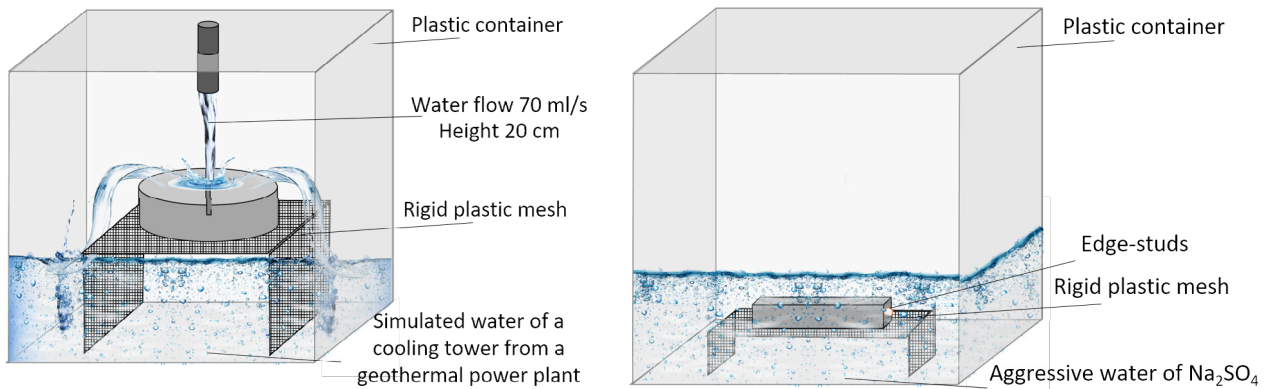


FIGURE 1. Set-up for the dynamic test (left) and the static test (right).

the water on the specimen. The test conditions aimed at promoting physical impact through the movement of the water itself, which was recirculated from the bottom of the plastic container to the top with a flow rate of 70 ml/s and impacted the sample from a height of 20 cm. The containers were topped up periodically to maintain a constant volume of the aggressive solution. The test was performed with three cracked and three uncracked samples of Ø100x50 mm per type of concrete. After 12 months, the dynamic interaction of the water was stopped for 2 months and restarted up to 24 months. Both the leachates of the simulated geothermal water and the concrete samples were analysed. The parameters analysed for the water leachates were: electrical conductivity, pH and ion content. The parameters obtained from the concrete specimens were: electrical resistance, changes in length and weight, SEM-EDX and crack mapping.

The static tests (Figure 1 - right), both in sulphate solution and in simulated geothermal water, were performed according to standard ASTM C1012-04. For each test, nine samples of 40x40x160 mm<sup>3</sup> equipped with two edge studs pre-inserted at the centre of the 40x40 mm<sup>2</sup> lateral surfaces were permanently immersed in the same aggressive water. The test with ss lasted 15 weeks, as stated in the standard, while the test with sgw was extended and lasted more than 550 days. The weight and length

of the samples were monitored periodically during the tests.

### 2.2.3 Crack generation

In a set of Ø100x50 mm samples, 5 mm notches were performed (Figure 2) and the samples were further cracked via the Brazilian splitting tensile test with a constant rate of 0.5 µm/s in order to obtain a single crack. The crack mouth opening displacement (CMOD) was controlled with an extensometer placed between two steel plates fixed on each side of the notch (Figure 2). The test was stopped so as to obtain maximum cracks around 50 µm, this meaning approximately 150 µm in the loaded state (Figure 2). After the test, the cracks were recorded and analysed at different points to determine the real crack widths on both surfaces of the sample. The initial cracks obtained for XA-CA (around 300 µm) were larger than those obtained in XA-CA+ANF and XA-CA+CNC (around 40 µm).

### 2.2.4 Parameters measured in the solution

The deionised water and the simulated geothermal water used in the dynamic test were analysed periodically to study their interaction with the UHP-FRCs with nanoadditives. The results from the tests

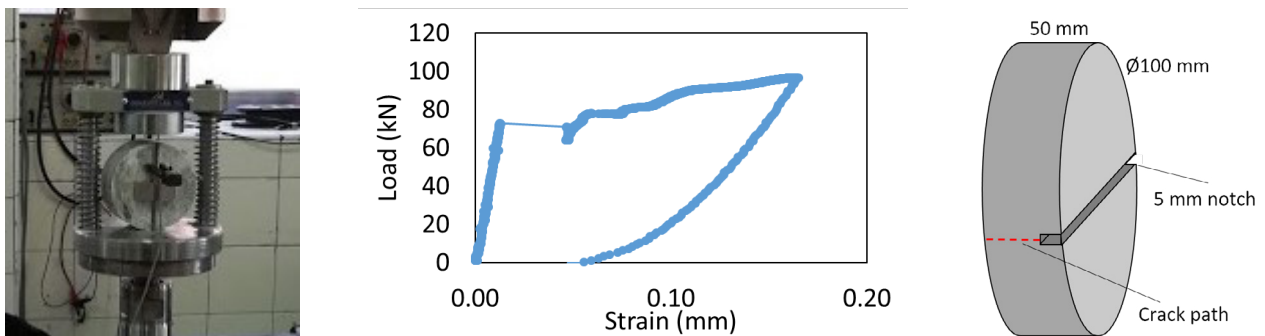


FIGURE 2. Splitting test of notched samples (left) and strain evolution during the test (right).

performed on cracked specimens were evaluated separately from those of uncracked specimens in order to identify the influence of the cracked state on the interaction between the concretes and the environment. Three parameters were obtained:

- pH and electrical conductivity were measured periodically using a multi-parameter instrument, the HI 255 Combined Meter (Hanna instruments).
- Ion content was characterised in the dynamic tests by analysing the changes in chemical composition over time in the dw and sgw. For this, aliquots were taken periodically and chemically analysed to detect the ionic evolution associated with the leaching phenomenon. For  $\text{SO}_4^{2-}$ ,  $\text{K}^+$ ,  $\text{Ca}^{2+}$  and  $\text{Na}^+$ , changes were analysed by inductively coupled plasma (ICP), while  $\text{Cl}^-$  was analysed by potentiometric titration.

Differences between both solutions were studied by comparing ion content (ppm) in the leachates of the deionised water and the difference between the ions measured periodically in the simulated geothermal water, normalised by the correction of the sgw ion content introduced during the test, as shown in Equation [1], in which  $\text{Ion}_t$  is the ion content measured in the leachates after  $t$  days of exposure and  $\text{Ion}_c$  is the initial ion content in sgw plus the corresponding ions added when topping up the volume with sgw, which are identified as real ions in the aggressive water or the no-ion interaction. Within the calculation, the periodic amount of sgw volume added to top up the containers ( $\text{Vol}_{add}$ , in l) was used to calculate the corresponding added ions ( $\text{Ion}_{add}$ , in mg) and were considered when calculating the real ion content ( $\text{Ion}_c$ ) in the leachates, according to Equation [2] and Equation [3].  $\text{Vol}_0$  and  $\text{Ion}_0$  are the initial volume (in l) and the initial ion content (in mg) of sgw respectively.

$$\text{Ion}_t - \text{Ion}_c \quad [1]$$

$$\text{Ion}_c = \frac{\text{Ion}_0 + \text{Ion}_{add}}{\text{Vol}_0 - \text{Vol}_{add}} \quad [2]$$

$$\text{Ion}_{add} = \frac{\text{Vol}_{add} \cdot \text{Ion}_0}{\text{Vol}_0} \quad [3]$$

To assess the influence of nanoadditives in sgw, the evolution was characterised by comparing each ion measured ( $\text{Ion}_t$ ) with the ion content corresponding to no-interaction taking into account the initial and the added ion content ( $\text{Ion}_c$ ). To facilitate comparing the effects on the different types of concrete,

the ratio ( $r$ ) was obtained according to Equation [4] through the values obtained for  $\text{Ion}_c$  and  $\text{Ion}_t$ , which corresponds to the ion content in one litre (ppm) of sgw at time  $t$ .

$$\text{ratio } (r) = \frac{\text{Ion}_t}{\text{Ion}_c} \quad [4]$$

Having determined the variation of  $r$  over time, an  $r > 1$  was considered to indicate that a leaching phenomenon was dominating for the respective ion, while an  $r < 1$  was considered to indicate the uptake of that ion by the cementitious matrix of the concrete, and an  $r \equiv 1$  indicated no relevant interaction.

### 2.2.5 Parameters measured on the concrete

To evaluate the influence of the environment, variations in weight were measured in both the static and dynamic tests, and variations in length were measured in the static tests. Additionally, the influence of cracks was studied by analysing crack evolution, electrical resistance and sample characterisation in terms of microstructure (analysis by scanning electron microscope with energy dispersive x-ray, SEM-EDX) after the exposure time.

- Length and weight: changes in weight were measured in both setups (dynamic and static) considering all three environmental conditions (dw, ss and sgw), while length was measured in the static tests for the ss and dw environmental conditions. Weight was monitored by weighing the samples periodically. Before weighing the samples, the surface was gently dried with a cloth, after which they were weighed with a precision of 0.01 g. Length was monitored in the prismatic samples by measuring the distance between the pre-inserted edge studs over time using a comparator with a precision of 0.01 cm.
- Electrical resistance was measured with an AUTOLAB 84750 potentiostat/galvanostat, using a pure sine wave AC voltage of 32 mV RMS at a frequency of 10 kHz. Two electrodes producing a uniform electrical current flow were connected to both sides of the cylindrical specimen, parallel to the crack propagation (Figure 3). Uncracked specimens were also measured to compare both results. For this reason, and due to the geometry of the samples, electrical conductivity cannot be calculated because surface measurements cannot be determined. Despite this, as electrical resistivity is directly proportional to electrical resistance when the measurement methodology is maintained and the geometry of the samples is the same, electrical resistance could also be used as a parameter.

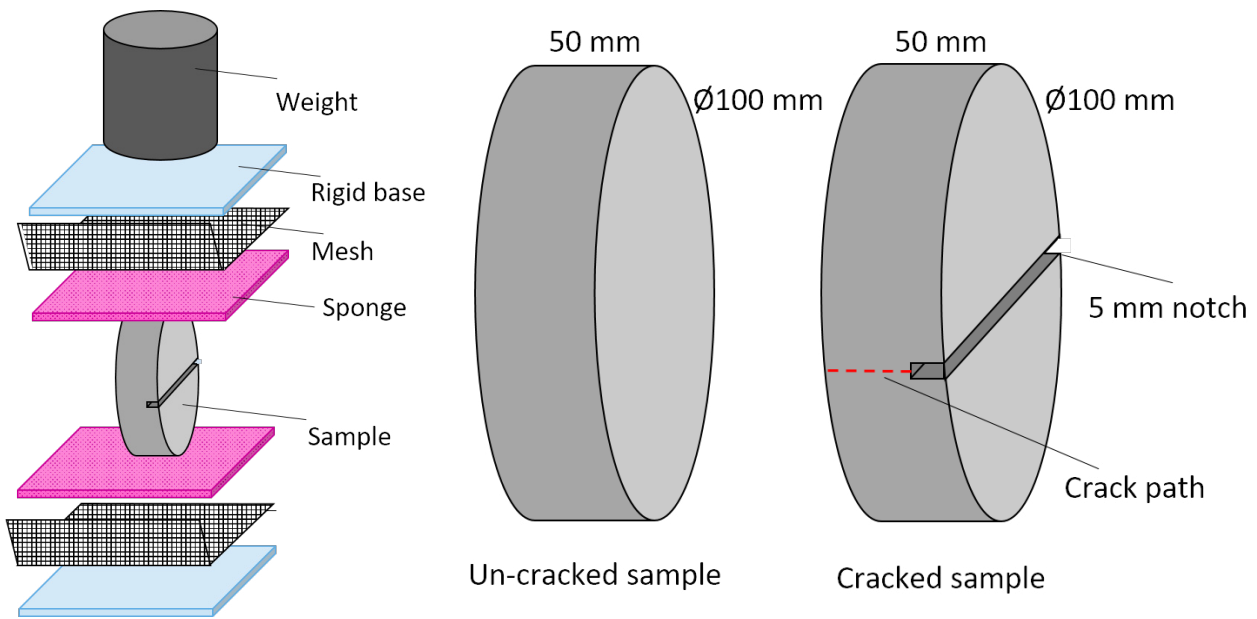


FIGURE 3. Electrical resistance scheme.

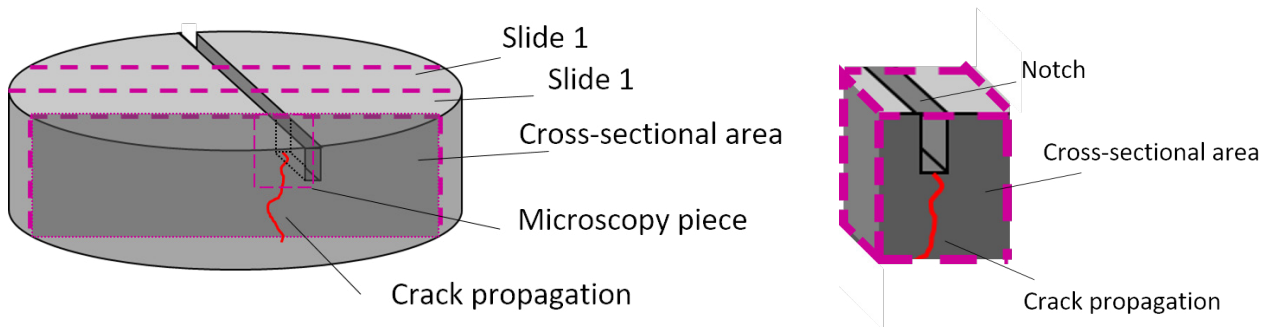


FIGURE 4. Diagram for obtaining samples for the microscopy piece (left) and microscopy piece (right).

TABLE 3. Parameters measured in the aggressive environments and type of aggressive interaction.

Concrete type	Aggressive interaction mode	Aggressive media characteristics	Parameters
XA-CA	Static	ss: 5 °C	Concrete: Length / Weight
XA-CA+ANF		sgw: 20 ± 2 °C	
XA-CA+CNC	Dynamic (water impact)	dw: 20 ± 2 °C	Water eluates: pH / Electrical conductivity / Ion content Concrete: Weight / Electrical resistance / Microstructure
		sgw: 20 ± 2 °C	

- Microstructure analysis by SEM-EDX: a Hitachi S-4800 scanning electron microscope was used in backscattered mode (BSEM), equipped with a BRUKER 5030 energy dispersive analyser set at 20 kV accelerating voltages and a beam current of 20 µA. To obtain the images, pieces of UHPFRC of around 20 mm were embedded into an epoxy resin and cut, polished and coated with carbon. The samples were stu-

died along their depth, considering pieces of uncracked concrete and pieces corresponding to the cracks in cracked samples to analyse the crack section. The pieces for microscopy were obtained from a slice of the sample cut crosswise to the crack (cross-sectional area in Figure 4). Figure 4 shows a diagram for how samples were obtained from which the microscopy pieces were extracted.

Analysis of the interaction of UHPFRCs with the aggressive media implies following the evolution over time of the chemical and physical parameters of the systems under study. Table 3 compiles the parameters measured in each aggressive environment (aggressive interaction type and medium) for each type of concrete.

### 3. RESULTS AND DISCUSSION

#### 3.1. Results

##### 3.1.1 Chemical interaction of UHPFRC with waters of varying compositions

Chemical interactions (ion leaching or uptake by the concretes) were studied through changes in the leachates in the aggressive media, measuring parameters such as pH, electrical conductivity and ion content. These parameters inform about the evolution

of the aggressive media and concrete characteristics due to dynamic interactions with dw and sgw.

Figures 5a and b show the evolution of pH due to sgw and dw interactions with cracked and uncracked UHPFRCs. The type of aggressive water evidently affects pH evolution and values, which are higher in the case of deionised water, stabilising at a pH of around 9.0. This increase in pH in the leachates is associated with the dissolution of alkaline phases and the release of alkaline ions into the water, as well as the initial pH of the solution, as was detected in previous studies (17, 20). Due to the lower initial pH in the case of sgw (see Table 2), stabilisation was achieved at lower pH values than in the case of dw, where the initial pH was higher. In addition, the tanks were topped up with fresh solution at pH = 3, which contributed to dampen the increase in pH. Despite this, the pH trends show a very similar evolution for both media. Figure 5b shows that although the initial pH of sgw was acidic (pH = 3), after only a few hours in contact with the UHPFRC the pH increased to around 8.4–8.5. Cracked samples show

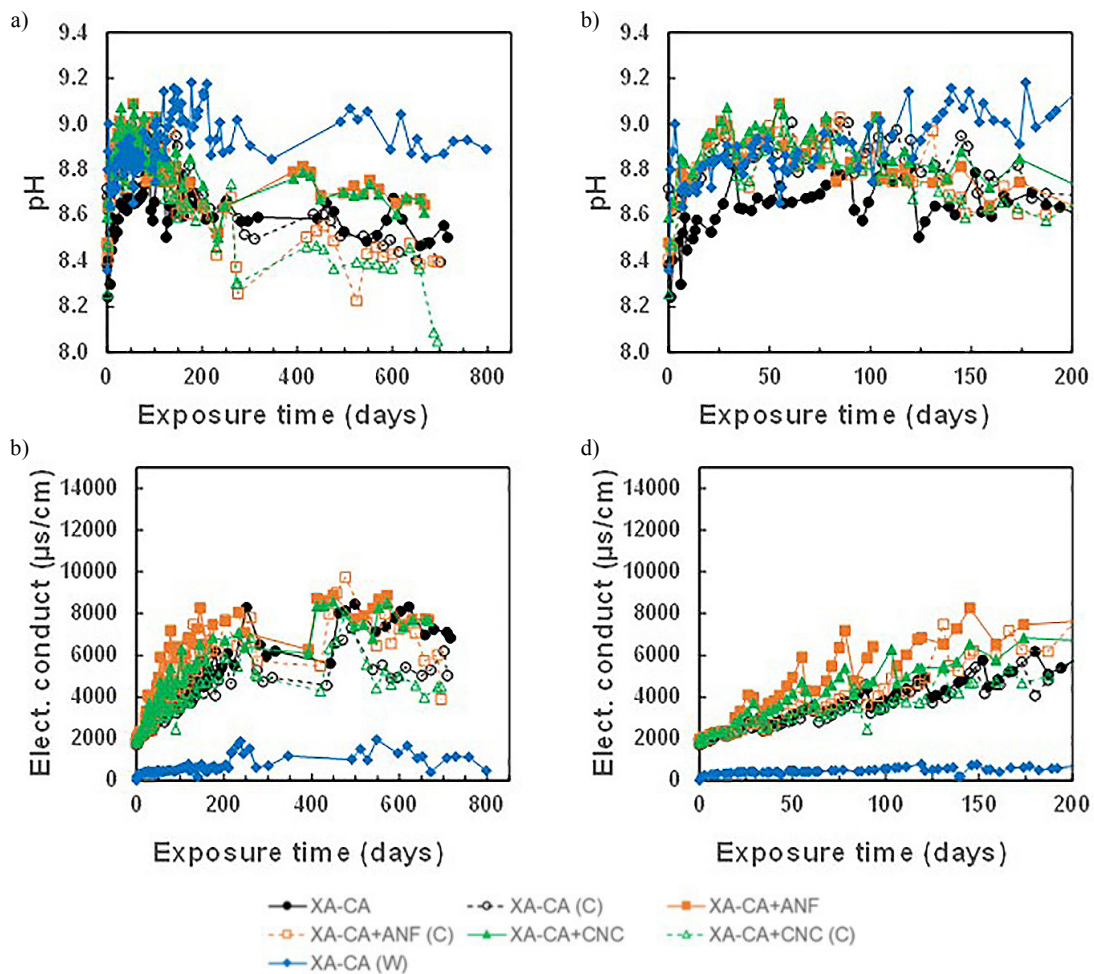


FIGURE 5. a, b) Evolution of pH, c, d) evolution of leachate electrical conductivity in uncracked and cracked concrete systems under dynamic water interaction in sgw and dw.

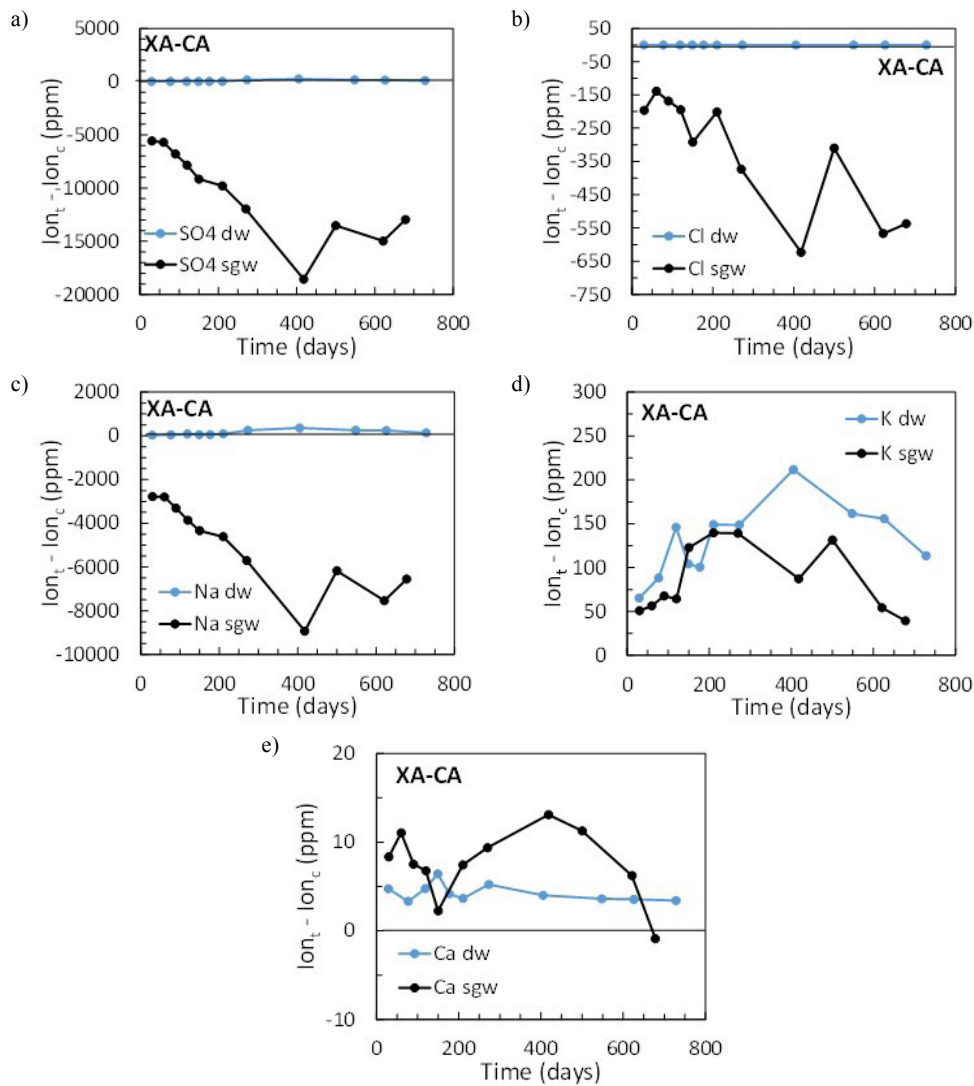


FIGURE 6. Chemical interaction in geothermal water versus deionised water: a)  $\text{SO}_4^{2-}$ , b)  $\text{Cl}^-$ , c)  $\text{Na}^+$ , d)  $\text{K}^+$  and e)  $\text{Ca}^{2+}$ .

a similar response during the first 200 days of exposure. However, some lower pH values were measured in longer exposures, and the response was similar in the three types of concrete (Figure 5a), with values within the mentioned range. Although no definitive explanation can be given to this difference between cracked and uncracked concretes, the response could be attributed to the local effect of the crack, which exposes a greater surface of the concrete and allows more interaction with the water, thus favouring, with longer exposures, the chemical conditions for the formation of solid phases inside the crack, as demonstrated later to have occurred.

The evolution of leachate electrical conductivity in the aggressive media, Figure 5c and d, informs about the presence and exchange of ions between the waters and concretes. Thus, there were no ions in the deionised water at the beginning of the test, while the starting point for sgw corresponds to the

ions present in the initial state of the simulated aggressive water, showing a clear difference between the two types of water. In both systems, electrical conductivity increased over time.

The chemical interaction between the aggressive media and the concrete was confirmed by comparing the initial and the measured values of electrical conductivity, so an increase in ion content is reflected through an increase in electrical conductivity and vice versa. The peaks obtained correspond to topping up the container with new solution to maintain the volume of solution in the container. Figure 5d shows an ascending curve during the first 200 days of interaction, which is more evident in the interaction with sgw, suggesting the incorporation of new ions to the leachates from the concrete due to a leaching process that is dominating the interaction. This period of increase is later accompanied by a period, until 600 days of exposure, of no relevant changes, followed

by a decreasing curve for longer exposures, associated with a decrease in the incorporation of ions to the leachates, probably with the simultaneous effect of decreased diffusion of ions from the interior of the concrete and the precipitation of solid phases on the surface of the concrete limiting the release of further ions. Electrical conductivity continuously increased during the test regardless of the type of concrete.

Cracked samples maintained the same evolution and trend in electrical conductivity related to concrete type and test stage. The same differences between concrete mixes are observed in the uncracked and cracked states. However, the values for cracked concretes remained slightly lower than those for uncracked specimens. The cause could be the healing of cracks with products that could come from the leached ions, as suggested by Cuenca *et al.* (46). Local differences in the chemical composition of water inside the crack with respect to that at the surface could have a relevant effect because water movement inside the crack is limited with respect to water movement on the surface.

The evolution of the ion composition of the leachate waters was analysed to evaluate the concrete-water chemical interaction at different ages, normalised by correction of the initial ion content in the water and the ions introduced during the test ( $\text{Ion}_t - \text{Ion}_c$  in ppm). To isolate the influence of water aggressiveness, sgw versus dw, the ions contained in the leachates for XA-CA concrete were compared, shown in Figure 6. In the case of dw, the concrete could not uptake ions, so all the curves remain at or above zero ppm.

Figures 6c and d show the effect of initial ion content for alkalis  $\text{K}^+$  and  $\text{Na}^+$  under both dw and sgw, with clear differences in response according to the type of ion. Figure 6c, corresponding to  $\text{K}^+$ , shows a progressive increase in content in the leachates for both dw and sgw, which suggests that this ion is leaching from the concrete. However, for  $\text{Na}^+$  an uptake is observed in sgw, compared to leaching in dw (Figure 6c). After 500 days, the ion content decreased in the case of  $\text{K}^+$  and increased in the case of  $\text{Na}^+$  (Figure 6d and c, respectively), probably due to an attenuation of the leaching process as observed in the electrical conductivity shown in Figure 5. In Figure 6e, the increase of  $\text{Ca}^{2+}$  content was measured in the leachate waters, although a smaller amount was determined in the dw, remaining practically constant over the entire exposure time. In sgw the trend in the evolution of  $\text{Ca}^{2+}$  suggests leaching of  $\text{Ca}^{2+}$ , followed by a progressive decrease, probably due to formation of some surface phases, such as calcite. A similar response was found in (17). Regarding sulphate, Figure 6a shows a depletion in the sgw solution, probably as a consequence of interaction with the concrete and the formation of compounds containing solid phases of sulphate, sulphoaluminate or ettringite. This was also suggested in (23). In the case of chlorides (Figure 6b), when the concretes

were in contact with the sgw, the interaction indicates a trend towards  $\text{Cl}^-$  uptake from the beginning and for the duration of the test.

### 3.1.2 Chemical interaction of UHPFRC including nanoadditives with sgw

The different types of concrete were compared using the ratio between the ions measured in the sgw leachates at different ages and the initial content of each ion, taking into account the topping up of the water tanks as explained in the experimental methods. The  $\text{Ion}_t/\text{Ion}_c$  ratio allows identifying the ion uptake capacity of each type of concrete with respect to the ions released to the exposure media.

Sodium ions (Figure 7c) were clearly below the initial content in the simulated geothermal water ( $r = 1$ ), thus confirming that an interaction with the concretes is taking place. However, no clear differences were appreciated regarding the type of concrete, so the solution analysis for this ion shows no influence for the type of nanoadditive used in the mix. With respect to  $\text{K}^+$  and  $\text{Ca}^{2+}$ , (Figure 7d and e, respectively), both ions were released from the cement paste, showing a ratio  $r > 1$  from the beginning of the test. However, the concentration trends along the exposure time were different and depend on the type of concrete. The  $\text{K}^+$  ratio shows a decrease in all cases, which then increased slightly after approximately 300 days of testing and stabilised at the end of the test. The ratio of  $\text{Ca}^{2+}$  ions decreased over time for XA-CA, with a greater concentration than those leached for the other two concretes at the beginning of the test (Figure 7e). On the other hand, XA-CA+ANF and XA-CA+CNC showed limited interaction during the first 150 days with some periods of  $\text{Ca}^{2+}$  uptake in the case of XA-CA+CNC. After the first 150 days the samples started the  $\text{Ca}^{2+}$  leaching process, with lower relative ratios than XA-CA, but finally reaching values very similar to the initial ratios showed by XA-CA or even higher in the case of XA-CA+CNC. After approximately 300 days of the leaching process, the curves approached stability at a ratio of 1, or slightly higher in the case of XA-CA+CNC.

Concerning the aggressive ions present in the sgw, the ratio of sulphates  $r < 1$  (Figure 7a) suggests interaction in all concrete types, probably as a consequence of the formation of insoluble compounds (23); some lower  $r$  values were detected in the case of XA-CA. Figure 7b shows an uptake of  $\text{Cl}^-$  ions from the beginning by XA-CA with a constant ratio, while in the case of XA-CA+ANF the uptake of  $\text{Cl}^-$  ions started later. This means that the uptake of ions from XA-CA+ANF and XA-CA+CNC was lower in comparison to XA-CA. This indicates some interaction with the cement paste of the concrete matrix, but also that the lower porosity of concretes with ANF and CNC affects the uptake of sulphate and  $\text{Cl}^-$  by such concretes.

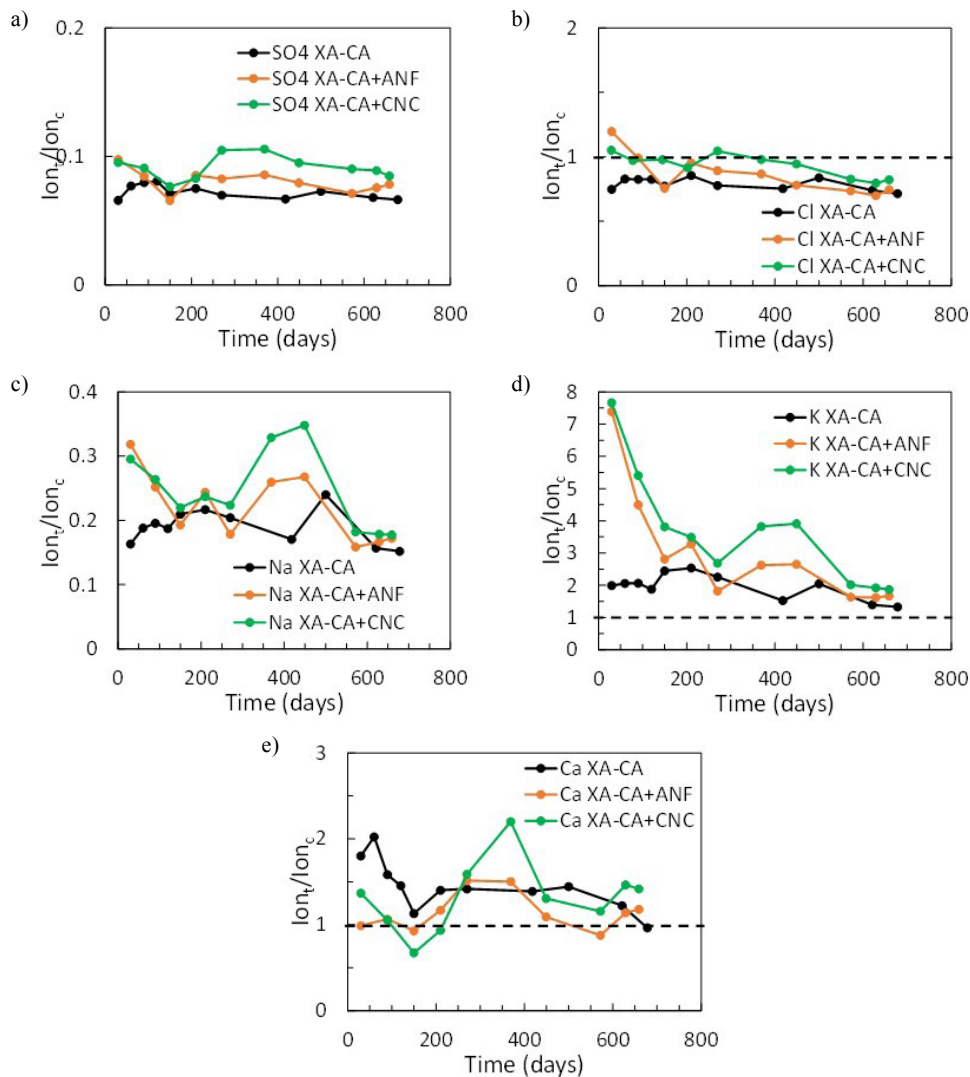


FIGURE 7. Leaching analysis from the XA-CA, XA-CA+ANF and XA-CA+CNC over time: a)  $\text{SO}_4^{2-}$ , b)  $\text{Cl}^-$ , c)  $\text{Na}^+$ , d)  $\text{K}^+$  and e)  $\text{Ca}^{2+}$ .

### 3.1.3 Interaction with the cement paste and new phase formation

The interaction of the aggressive medium with the cement paste in UHPFRC was studied to identify the formation of new solid phases and changes in the microstructure of the cement paste. First of all, a visual inspection was carried out in order to locate surface damage due to the exposure conditions in cylinders subjected to the dynamic water test with sgw. The concrete surface did not appear significantly altered, but precipitates on the surface in all concretes and steel fibres showed corrosion (Figure 8).

Furthermore, a study was performed using SEM/EDX comparing the compositions at different depths from the surface to the concrete bulk. The results of this study were compared with the initial microstructure of the UHPFRCs before testing. Additionally, in the case of cracked concretes, the crack section

was studied to identify the interaction of this part of the sample with the sgw. Although both cracked and uncracked samples were subjected to the same test conditions, the local effects in the crack area were different from those of the surface area because water movement and renovation is limited.

The main oxides composition of the cement paste for the three UHPFRCs studied before being exposed to the sgw (Figure 9 left), showed that the concretes have a compact matrix phase, showing anhydrous cement particles and unreacted slag grains. A homogeneous C-S-H gel was the main hydration product. The main oxides that constituted the C-S-H were  $\text{CaO}$ ,  $\text{SiO}_2$  and  $\text{Al}_2\text{O}_3$  (Figure 9 right). The three UHPFRCs presented similar  $\text{SiO}_2$  and  $\text{Al}_2\text{O}_3$  percentages, around 24.3% and 6.7% respectively, which indicates the incorporation of Al into the C-S-H, as observed by previous authors (17, 47). However, a certain difference in CaO content was detected be-

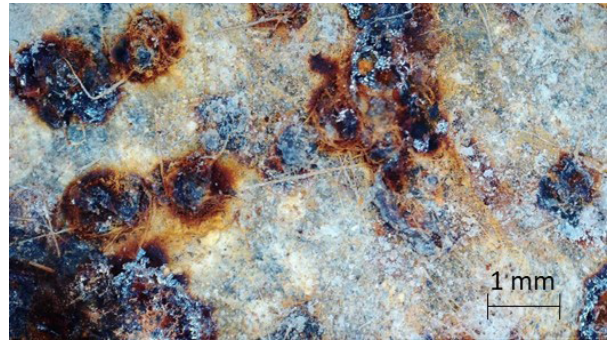
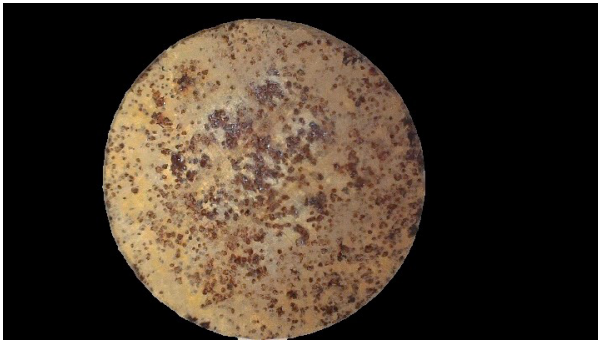


FIGURE 8. Surface inspection. Example of XA-CA+ANF fibre corrosion.

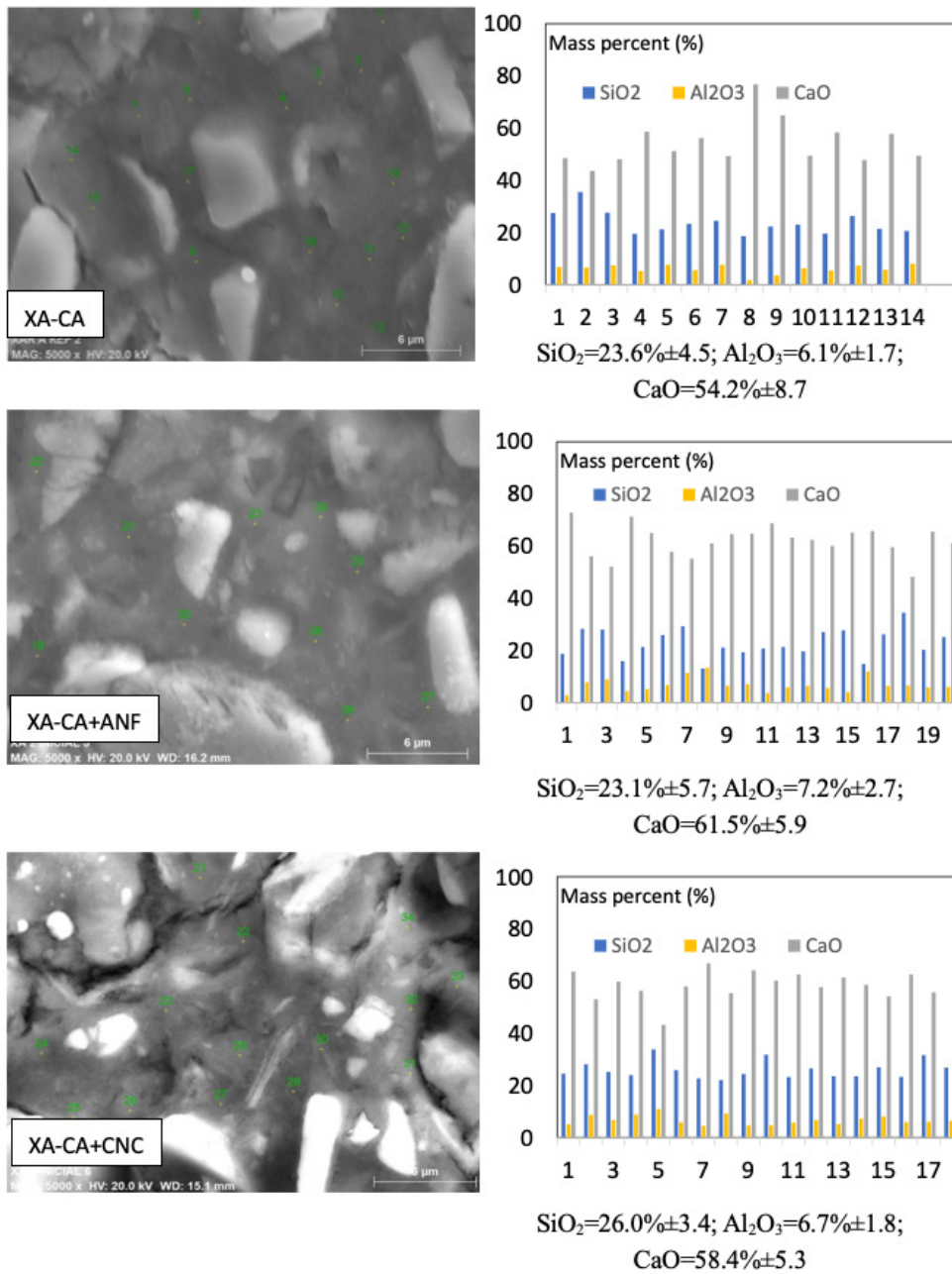


FIGURE 9. SEM/EDX study of the UHPFRCs XA-CA (top), XA-CA+ANF (middle) and XA-CA+CNC (bottom).

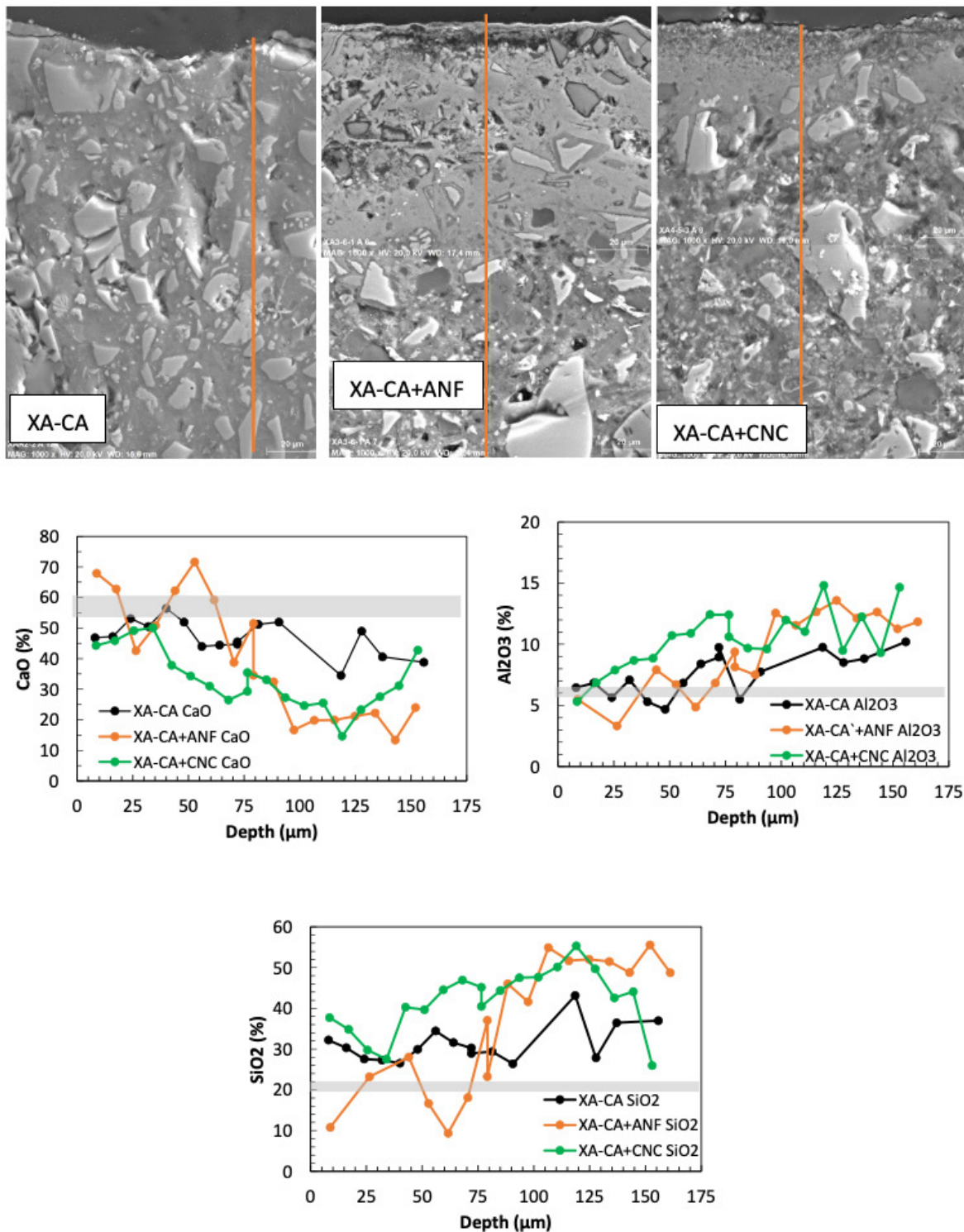


FIGURE 10. SEM/EDX depth study (top) and chemical composition (bottom) of the UHPFRCs XA-CA, XA-CA+ANF and XA-CA+CNC.

tween them, from 54.2% to 61.5% depending on the type of UHPFRC, with XA-CA concrete presenting the lowest percentages. The presence of BFS favoured the incorporation of Al in the cement pastes as in conventional concretes (17).

Figure 10 shows the microstructure and chemical composition at different depths from the surface on which sgw impacted the three UHPFRCs after 24 months of exposure. XA-CA (top) presented a homogeneous matrix from the surface to the concrete

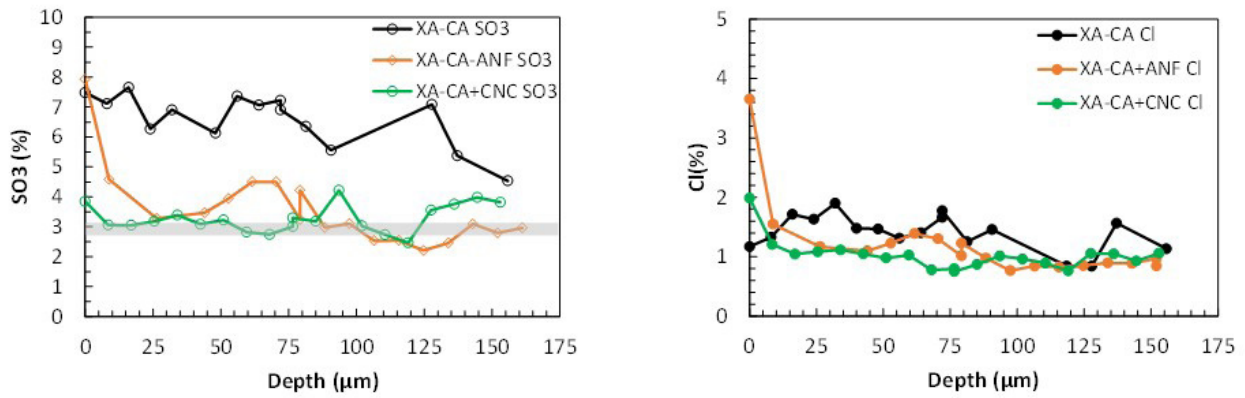


FIGURE 11. SEM/EDX depth study of Cl and SO<sub>3</sub> in UHPFRCs with nanoadditives.

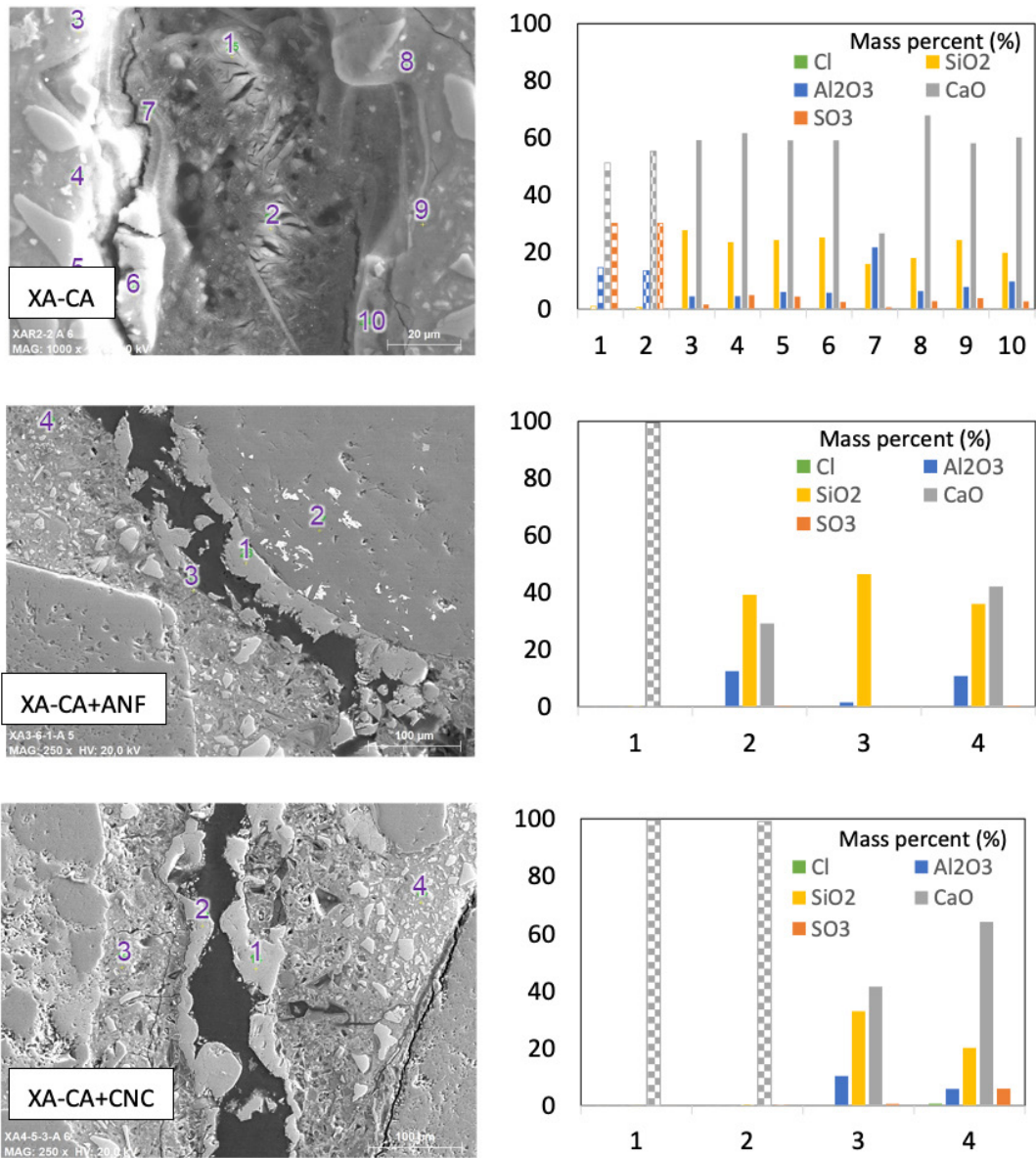


FIGURE 12. Interactions in cracks of nanoadded UHPFRCs with the simulated geothermal water after the test and SEM/EDX study of the crack section in XA-CA (top), XA-CA+ANF (middle) and XA-CA+CNC (bottom).

bulk (150  $\mu\text{m}$  in depth). On the surface, a smaller number of anhydrous cement and slag particles were observed in comparison with the XA-CA matrix before testing (Figure 9). The anhydrous grains in direct contact with the water were hydrated, developing C-S-H gel and compacting the system. The chemical composition of the cement paste at different depths is evaluated in Figure 10, bottom, which shows the initial chemical composition of the concretes with a grey band.

Micrographs of the XA-CA+ANF and XA-CA+CNC concretes clearly show two zones (Figure 10, top). The first of these was continuous and compact, with a thickness of 80  $\mu\text{m}$  for the concrete including ANF and 42  $\mu\text{m}$  for the concrete with CNC. This zone was characterised by being rich in CaO and low in  $\text{SiO}_2$ , probably corresponding to calcite formation. The second zone had a more similar appearance to that observed in XA-CA, where a highly densified matrix with few unreacted raw materials was observed. However, the chemical composition is different, suggesting silicon enrichment and calcium depletion, achieving values of 50%  $\text{SiO}_2$  and 24% CaO.

The aggressiveness of the sgw environment does not only cause leaching. Due to the presence of sulphates and chlorides, the concretes can also induce alteration of the cement paste. Figure 11 shows the evolution with depth of Cl and  $\text{SO}_3$  in the three nanoadded UHPFRCs after 24 months of exposure, including the initial content as a grey band. Chlorides show a certain penetration profile in the three types of concrete – clearer in the case of XA-CA+ANF and XA-CA+CNC – along the first 150  $\mu\text{m}$  studied from the surface, although percentages did not exceed 4%. Sulphates also show a clearer profile in the case of XA-CA and XA-CA+ANF.

When cracks were present, differences were observed with type of concrete. Some precipitates of a different nature appeared throughout the crack surface as observed in Figure 12, which shows the crack section of three concretes (XA-CA, XA-CA+ANF and XA-CA+CNC) after 24 months of exposure. In

the case of XA-CA, the crack appeared to be slightly covered by a precipitate covering most of the crack. It was a calcium, aluminium and sulphate-rich compound identified as ettringite, while XA-CA+ANF and XA-CA+CNC presented a denser precipitate on the walls of the crack, consisting mainly of a calcium-rich phase which did not fill the crack homogeneously. This confirmed the interaction between the crack surface and the medium after 24 months of exposure, although the cracks were not totally filled by these precipitates. In all cases, despite the different morphology of the precipitates, the concrete bulk remained stable, with no variations in chemical composition nor interaction with the aggressive medium. Despite the entry of chloride detected in all concretes, no solid phase related to Friedel's salt was identified in the concrete or the crack surface.

### 3.1.4 Response of UHPFRC in physical interactions with different aggressive water compositions

The samples suffered physical damage on their surface due to the impact and movement of the water, together with the chemical attack due to the aggressiveness of the water.

The variations in length measured in the static tests, both with ss and sgw, are presented in Figure 13. In the static test with ss, changes in length were observed in the three concretes during the first three months, regardless of the presence or absence of nanoadditives (Figure 13 left), with a deviation for XA-CA in the first 50 days. Volume stability was reached after 100 days of exposure, with slightly smaller values for XA-CA (Figure 13 right). The results obtained using sgw during the exposure time of 2 years are shown in Figure 13 right. An increase in length is detected over the first days, associated with water capture, no matter what nanoadditive was included in the concretes, as observed for ss. The variations in length later stabilise. Nevertheless, differences between concrete compositions were clearer during longer exposures due to differences

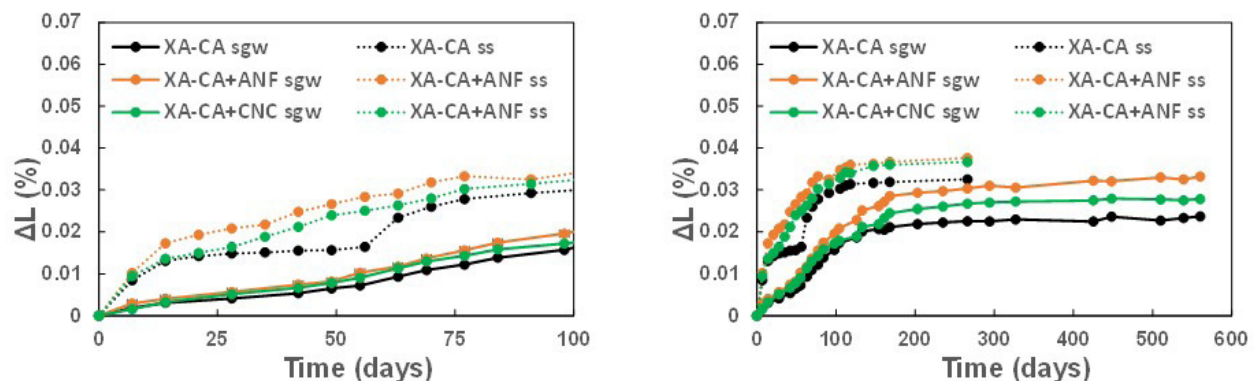


FIGURE 13. Change in length over time for XA-CA, XA-CA+ANF and XA-CA+CNC subjected to the static test with ss and sgw until 100 days of exposure (left) and until the end of the test (right).

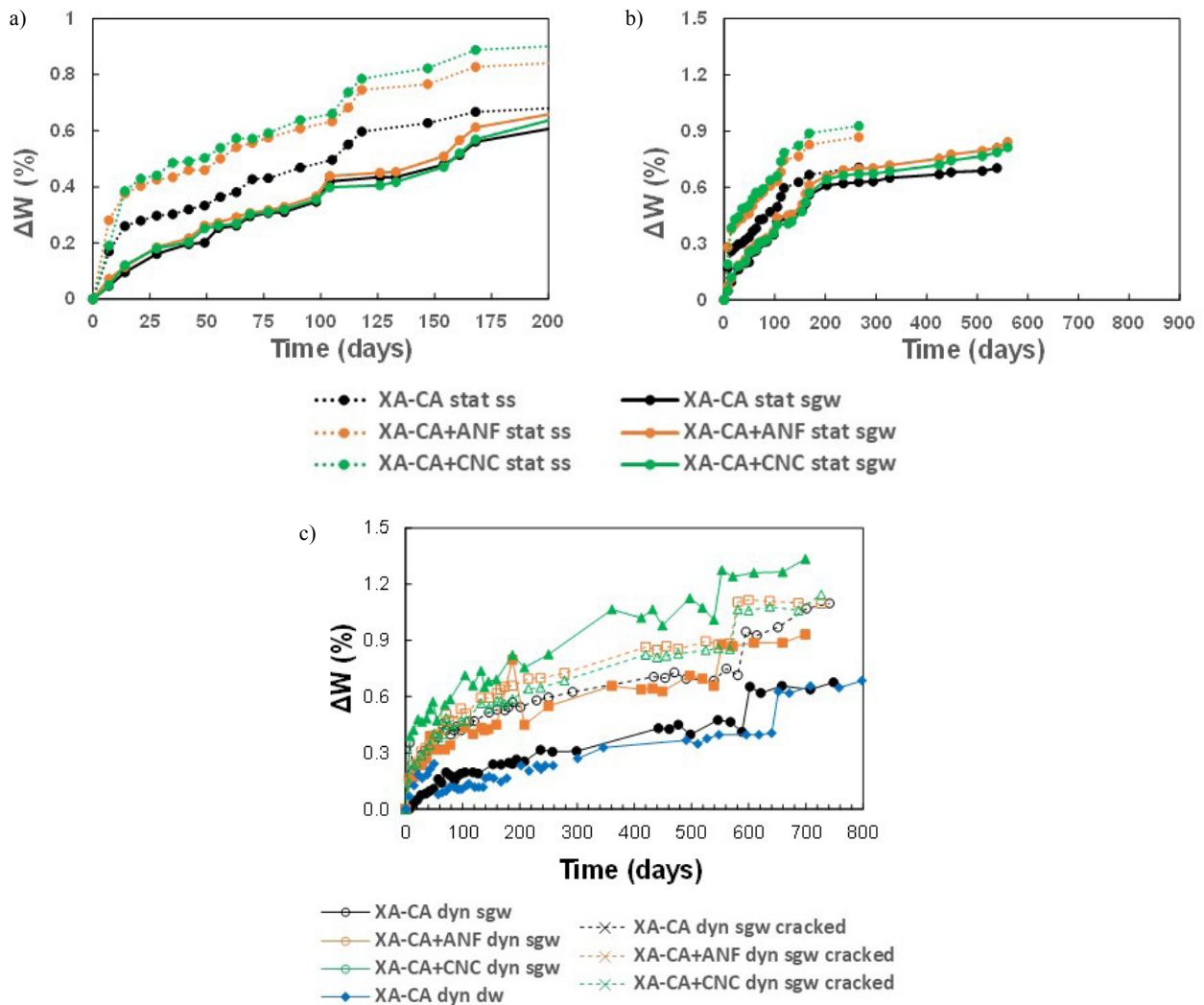


FIGURE 14. Changes in weight over time for XA-CA, XA-CA+ANF and XA-CA+CNC subjected to the static tests (a, b), and the dynamic test (c in sgw and dw).

in the water uptake of concretes including different additives. This was higher in concretes including CA+ANF and CA+CNC, although in all concretes the total  $\Delta L$  was negligible, below 0.04%.

Responses to both aggressive waters follow a two-stage response. The change in trend from the first increase stage to stabilisation showed a mismatch of around 50 days between the ss and sgw tests. However, the maximum variation reached is higher with ss at the end of the second stage regarding the static test with sgw. XA-CA showed the least changes in all test conditions.

Changes in weight are shown in Figure 14, corresponding to the same static tests in ss and sgw media and the same dynamic test conditions between dw and sgw. The dynamic tests in sgw also include information for cracked specimens.

In the static test with ss, the differences between types of concrete could be detected from the beginning, with a lower increase in XA-CA than in XA-

CA+ANF and XA-CA+CNC, which grew with very similar ratios (Figure 14a). This could probably be due to the higher water uptake of CNC and ANF nanoparticles suggested by Kawashima *et al.* (45). Despite this difference, the response in all mixes was very similar, maintaining the same slope in all the curves, which indicates that the growth rate in weight was similar (Figure 14b) showing the same two-stage behaviour, with lower rates during the second stage. In the static conditions with sgw, all concretes presented the same two-stage behaviour with a very similar ratio from the beginning regardless of the additives used (Figure 14c). However, during the second stage, the concretes with ANF and CNC increased in weight slightly faster than samples made of XA-CA concrete, which showed a more stable behaviour, as occurred in the static test conditions with ss.

In the dynamic test with sgw (Figure 14c), XA-CA concrete was the most stable, as in the static

tests, although in this case the differences in ratio observed in the curves were higher than those observed in the static tests, especially during the first period. In fact, the XA-CA growth ratio was constant from the beginning (excluding the first phase). This could also be caused by the water absorption capacity of the additives. However, in comparison to the static test, although a rapid increase was also identified, the curves do not follow the two-step shape; instead, there was a gradual change from the first slope to the final slope.

Although more pronounced in the cracked state, concretes gained weight over time with a similar ratio to the uncracked specimens in the case of XA-CA+ANF and XA-CA+CNC. In the case of XA-CA, samples gave rise to curves similar to those of the concretes functionalised with ANF and CNC.

In contrast, differences concerning the type of environment stand out in the dynamic test, with no weight variations in the concrete under the effect of dw. This leads us to affirm that the water movement and surface impact in this test is not sufficient to cause erosion and did not affect the weight stability of the concretes, but rather that erosion was caused by the chemical interaction of the aggressive ions in the water.

Electrical resistance was measured in both cracked and uncracked samples under the effect of the dynamic sgw, and is reported in Figure 15 along with the results obtained from the dynamic test with dw. The measurements were taken perpendicularly to crack propagation in order to detect possible effects due to the presence of cracks. Differences between concrete types were not remarkable, only XA-CA+ANF increased its electrical resistance for a period but rapidly converged to the mean resistivity of the uncracked concretes. An increase in electrical resistance could be related to a material with more defects such as cracks, pores, other internal defects or different densities. In this sense, cracked concretes are expected to give rise to higher values of electrical resistance than uncracked samples. This can be observed in Figure 15, in which the curves corresponding to cracked specimens (cr) appear slightly above the curves of uncracked specimens.

The samples subjected to the effects of deionised water showed similar electrical resistance, so we could confirm that media aggressiveness does not significantly affect the electrical conductivity of the concretes. In general, the results of electrical resistance over time remain more or less constant, showing no increasing or decreasing trends, which agrees with the volume stability of the concretes.

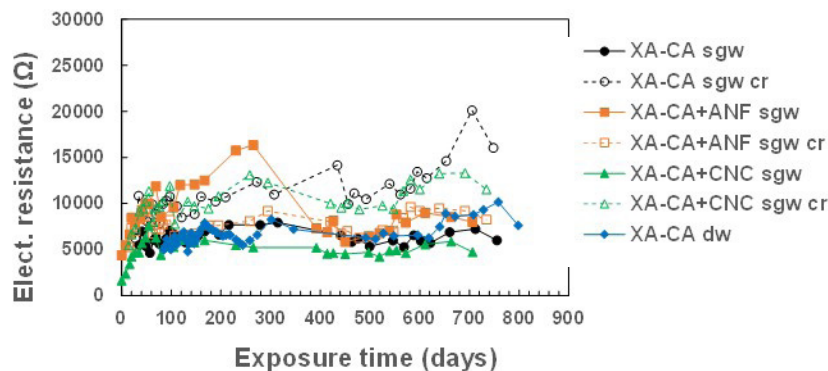


FIGURE 15. Electrical resistance over time for XA-CA, XA-CA+ANF and XA-CA+CNC subjected to the dynamic tests.

TABLE 4. Assessment of the influence of the different media, cracking and nanoadditives.

UHPFRC Durability Assessment	Two-by-two test comparison		
	sgw dynamic vs. sgw static	sgw static vs. ss static	dw dynamic vs sgw dynamic
Environmental boundary conditions	Convection regime (weight change)	Water composition and T effect (weight/length)	Water composition effect (Weight, pH Electrical conductivity Ion content)
Cracked state		-	Weight pH Electrical conductivity Microstructure
Characteristics of Nanoadditives	Length/Weight/pH/Electrical conductivity/Microstructure		

### 3.2 Discussion

The durability of concretes due to their interaction with aggressive waters depends significantly on the characteristics of the concrete and the composition and convection regime of the environment. In the present paper, several parameters were selected and evaluated separately. A joint analysis of the measured parameters was performed in order to assess the influence of the media, the cracking effect and the inclusion of nanoadditives. This analysis is presented below.

In order to discern the influence of each factor, the testing conditions were compared two by two, isolating the studied effect within each parameter and combining the partial conclusions to deduce the influence as a whole of the media, the cracking and the inclusion of nanoadditives. Table 4 shows the scheme followed for the analyses.

#### 3.2.1 Durability Response of UHPFRCs due to environmental boundary conditions

Aggressive media have been shown to affect the durability of UHPFRCs in different ways according to the aggressive exposure classes. This work compares two aspects of this influence of the media: the aggressiveness of the media due to its chemical composition (dw/ss/sgw) and due to its kind of interaction (static/dynamic).

To identify each effect, the influence of both aspects should be isolated taking into account the same boundary conditions: temperature, type of samples and concretes, type of test, parameter, and type of aggressive solution or aggressive interaction. Thus, to assess the influence of the media, the dynamic tests with dw and sgw were compared in order to detect the effect of the sulphate rich environment and the static tests were compared to detect the impact of aggressiveness. In addition, the dynamic and static tests with sgw were collated to identify the impact of water movement (Table 4).

- Influence of the media due to convection regime

The conditions of the simulated water impact regime were significantly less aggressive than those of the real situation in the geothermal plant (water impact from 20 cm vs 10 m), so that the convection regime followed was not aggressive enough to cause erosion (detected by weight loss) as occurs in a real exposure scenario. However, the higher resistance to physical impact offered by UHPFRCs can significantly contribute to a good response. Instead of weight loss, a weight gain was observed, as commented in Figure 14, that suggests an increased chemical interaction with the water components. This is in line with the findings of some authors (17) who compared tank water test and running water

test conditions on UHPFRC. The concretes in the dynamic regime showed higher growth than in static conditions in the sgw aggressive medium composition. Although the dynamic system was not a promoter of the interaction, the synergy between the aggressiveness of the media and the water movement resulted in a detrimental effect on sample stability. Although differences in the resulting damage were related to the type of physical interaction, as found by some authors using natural immersion and dry/wet cycles (49, 50) the dynamic state used acted as an aggravating agent but did not cause damage by itself.

- Influence of the media due to chemical water ion composition and temperature

The water composition had a significant influence on its interaction with the concrete. In the case of low ionic waters, the main effect of the chemical interaction is leaching if the convection regime does not cause any additional damage, as mentioned above.

Considering all the parameters analysed in the dynamic tests, the most selective durability indicator of aggressiveness and damage was that of ion changes in the leachates. On the other hand, other parameters such as pH partially inform of the effects of the aggressive. The leaching phenomenon caused by the media, sgw vs dw, overlaps with the interaction of ions that may penetrate the concrete matrix and react forming new phases that are more or less stable, and which also cause instability in the system. Figure 16 shows the accumulated ion content of XA-CA under the effect of dw and sgw, respectively. The leaching effect is higher for dw than for sgw (Figure 16a and b). However, the  $\text{Ca}^{2+}$  ion content in the leachates is considered a clear indicator of the leaching resistance of concrete in aggressive media in agreement with that proposed by (17, 20), which is one order of magnitude higher for sgw than for dw.

In the case of anions, the interaction was well identified for sgw, leading to the uptake of sulphates and chlorides as can be clearly deduced from Figure 16c. In both cases, dw was not affecting the concrete because it was an ion-free solution.  $\text{Cl}^-$  and  $\text{SO}_4^{2-}$  both penetrated the concrete, but the uptake of sulphates was noticeably higher than that of chlorides for the type of UHPFRC used in this study, reaching 32 times higher accumulated values, probably due to the initial higher content in the solution (2300 ppm of  $\text{SO}_4^{2-}$  vs 300 ppm of  $\text{Cl}^-$ ). The absence of Friedel's salt could be related to this higher sulphate content, although neither Friedel's salt nor ettringite were observed in the samples. This was also confirmed in the relationship observed between the oxides in the concrete, which was not aligned with any of these phases. Despite this, the higher uptake of sulphates suggests that intermediate phases could be forming, but further and more specific studies are needed

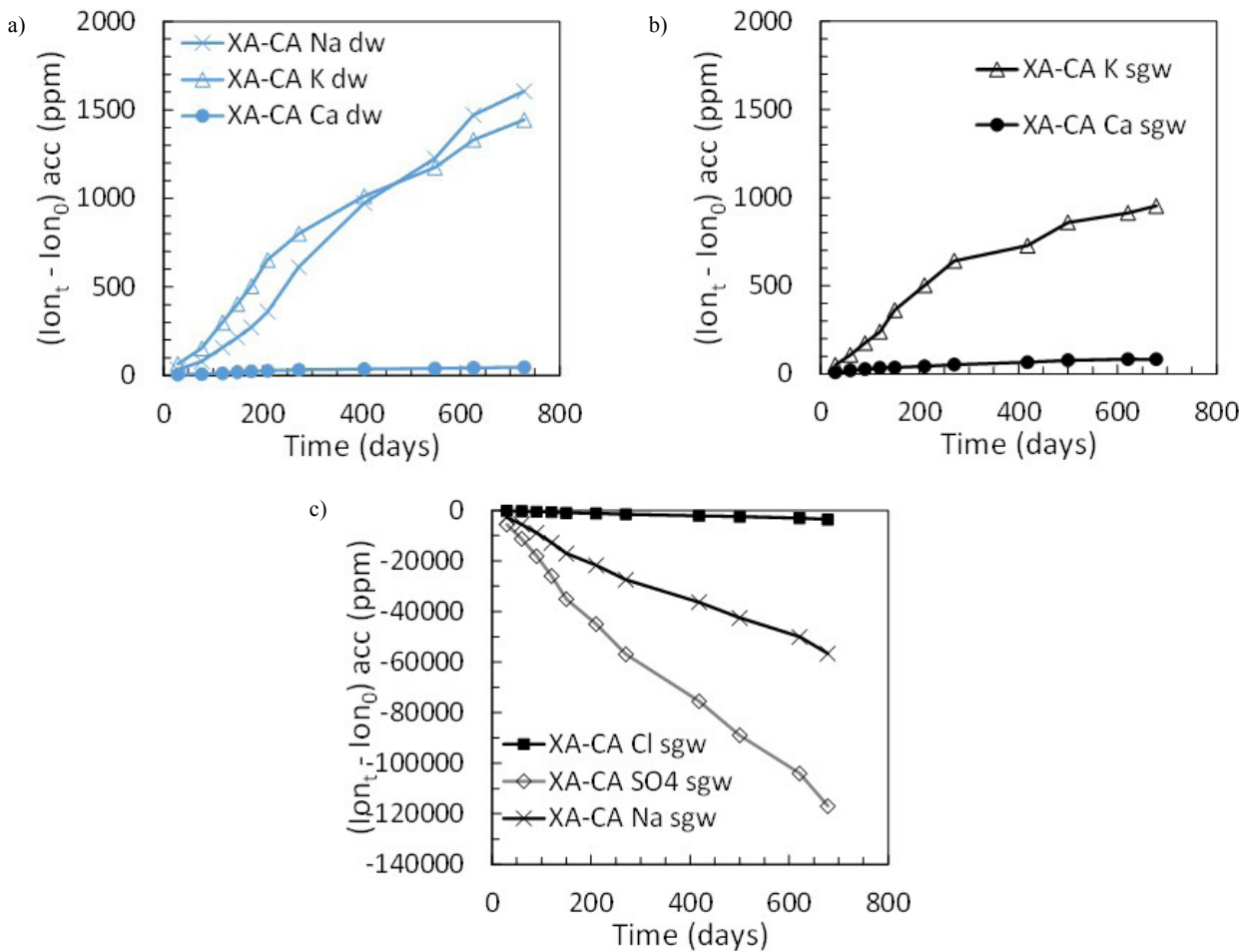


FIGURE 16. Accumulated ion content of XA-CA exposed to dw and sgw.

TABLE 5. Influence of each medium.

Influence of medium	Durability indicators of damage	Selective information
Due to convection regime (static vs. dynamic)		Higher in dynamic than in static conditions.
Variation in concrete weight		Water movement acts as a damage accelerator but not self-promoter.
Due to water composition (dw vs sgw)	Ion leaching, electrical conductivity	Non-remarkable information and selectivity. sgw leads to higher conductivity, suggesting more interaction.
	Variation in concrete weight	Higher aggressiveness of sgw influence regarding dw, which has almost no effect.
	Content and type of leaching ion	dw and sgw leachate alkalis. sgw leaches more $Ca^{2+}$ and leads to a chloride and sulphate interaction.
Due to testing temperature + water composition	Variation in concrete weight	No effect on response.
	Variation in concrete length	Slightly influences stabilisation levels.

to confirm this. In addition, not only chlorides and sulphates were penetrating the concrete, but also sodium, probably caused by the ion content of the solution (1280 ppm at the beginning of the test). Conversely, calcium was being leached in order to balance out the charges of the ions and to induce

stability in the system. This was also observed in the microscopy study, in which the solid phases showed lower content due to the leaching of calcium. The evolution of pH trending towards higher values confirmed the charge equilibrium because of the release of  $OH^-$ .

TABLE 6. Influence of cracking.

Influence of cracking	Durability indicators of damage	Selective information
On the leachate (sgw)	Leaching electrical conductivity	No remarkable information.
On the concrete (crack width)	Crack microstructure	Cracks not totally sealed. The precipitates differ depending on the width of the crack and changes in the local environment inside the crack.
	Variation in concrete weight	Not a good damage indicator.

Regarding the effect of temperature in conjunction with water composition, the static tests performed included ss at low temperature (5 °C) and sgw at 20 °C. The parameters studied in both conditions were the changes in length and weight of the concrete samples. Both showed the same two-stage behaviour, with similar points of inflection. So, aggressiveness due to water composition and temperature did not affect the behaviour as water composition and movement did. Although the response was maintained, the effect of water composition and temperature affected the stabilisation level of both parameters, with higher values observed in the static test including ss at the end of the exposure time.

Table 5 summarises the influence of the medium on the durability indicators studied and the type of aggressive interaction (dynamic or static).

### 3.2.2 Durability consequences of cracks in UHP-FRC

Cracking is common in working concrete structures, which results in a weak point for durability responses because cracks favour the ability of the aggressive to penetrate and interact with the concrete, as suggested in previous studies (18, 27, 28). However, the mechanism of interaction inside a crack is far from understood.

The hypothesis behind this study was to analyse if the interaction of the crack front changes with crack depth due to local changes in the composition of the water filling the crack. The lower pH observed in cracked specimens could be related to this fact due to the formation of precipitates.

Differences were observed at different crack depths that support the above hypothesis regarding water composition inside the crack, as well as the effect of water impact, which empties the upper part of the crack. This effect also seems to depend on crack width, which was wider in XA-CA (300 µm) than in XA-CA+ANF or XA-CA+CNC (40 µm). The inner part of the cracks did not show the same precipitates in all concretes, as was observed in the microscopy of the crack section. The Ca-rich precipitates observed inside the cracks vary

along the crack. Differences in chemical composition inside the crack can explain the differences in the interaction response of the crack front with the water inside the crack and precipitated compounds that seal the crack. Besides, wider cracks favour the penetration of sulphates and their interaction with the concrete, reaching conditions of chemical equilibrium that precipitate ettringite, while smaller cracks only showed the formation of Ca-rich compounds associated with calcite formation. Although this evidence was found in the present work, more studies are needed regarding the interaction of the crack with the aggressive water along the crack depth. Thus, the increase in weight observed in cracked specimens can be related not only to the capture of water but also to the interaction with aggressive ions in the medium and the formation of new solid phases such as ettringite within the cracks.

Table 6 summarises the influence of the cracked state on the durability indicators considered and their selectivity in the damage assessment obtained from the sgw and the concrete measurements in the dynamic test.

### 3.2.3 Influence of nanoadditives on UHPFRC durability

The effect of additives on different concretes was analysed regardless of test conditions or cracked state.

Variations in length and weight of XA-CA were the most stable. The higher increase in weight experimented by XA-CA+ANF and XA-CA+CNC could be due to water uptake by the additives, especially in the case of CNC. The cellulose fibres can be dispersed in hydrated cement paste and have the capacity to absorb and release water, so they provide internal curing (45). Despite this, the trend was maintained among the concretes.

The surface showed a Ca-rich layer in the case of XA-CA+ANF and XA-CA+CNC concretes, and this could be acting as a protection layer and be causing the damping of the weight increase after the first period in the dynamic test. Consequently, the interaction of the concrete with the medium diminished and the parameters tended to stabilise

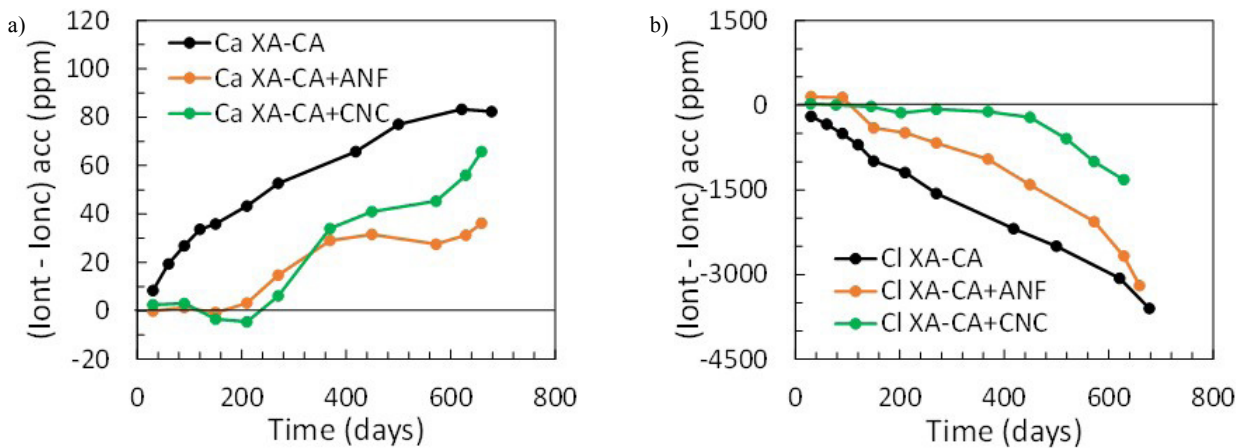


FIGURE 17. Accumulated ion content of XA-CA, XA-CA+ANF and XA-CA+CNC.

TABLE 7. Influence of nanoadditives.

Influence of nanoadditives	Durability indicators of damage	Selective information
Static	Variation in concrete length	Two-stage process Lower weight gain in XA-CA
	Variation in concrete weight	No remarkable information
Dynamic	Variation in concrete weight	XA-CA is the most stable XA-CA did not experiment increase + stabilisation
	Ion content	XA-CA is more affected by Ca leaching and Cl entrance and sulphate uptake
	Concrete characteristics and crack width	Superficial Ca-rich layer in XA-CA+ANF and XA-CA+CNC, higher in XA-CA+ANF Ca precipitates in XA-CA+ANF and XA-CA+CNC cracks Ettringite precipitates in XA-CA cracks

during the second phase (17). This layer is higher in the case of XA-CA+CNC, probably because CNC is acting as a hydration promoter (Figure 17). A similar Ca-rich layer was observed in a previous study (17).

According to the microstructural changes observed within the cracks, not only the appearance but also the chemical composition of the precipitates differed from XA-CA to XA-CA+ANF and XA-CA+CNC, these being ettringite and calcite respectively. Ettringite formation is observed, although the delayed ettringite formation is a known expansion problem that can promote microcracking (26, 51, 52). Over the period evaluated, calcium sulphoaluminate phases grew in the crack, and clear profiles of sulphate and chlorides were detected in the uncracked region (Figure 10 and Figure 11), which confirm penetration into the matrix and the corresponding decrease in the leaching media with no microcracking associated with their formation. A similar response was also observed in the interaction of conventional concrete in contact with sulphate- and chloride-rich

bentonite after 13 years of interaction with underground waters (25).

Furthermore, the analysis of the sgw ion composition showed a similar behaviour in general. Some differences were observed in the case of Ca<sup>+</sup> release (Figure 17a), with higher release in XA-CA, probably related to a higher porosity and the absence of the protective layer. The inactivity during the first 200 days in the case of XA-CA+ANF and XA-CA+CNC could be related to the formation of precipitates, which consisted mainly of CaO in both concretes. In the case of ion uptake, XA-CA is clearly more affected than XA-CA+ANF and XA-CA+CNC regarding chlorides, as is observed in the accumulated ppm represented in Figure 17b. XA-CA+ANF and XA-CA+CNC were more resistant to chloride penetration, especially when the inclusion of CNC clearly delayed the uptake that could also be related to its lower porosity.

Table 7 summarises the influence of the inclusion of nanoadditives in the UHPFRCs regarding the parameters studied in the dynamic and static tests.

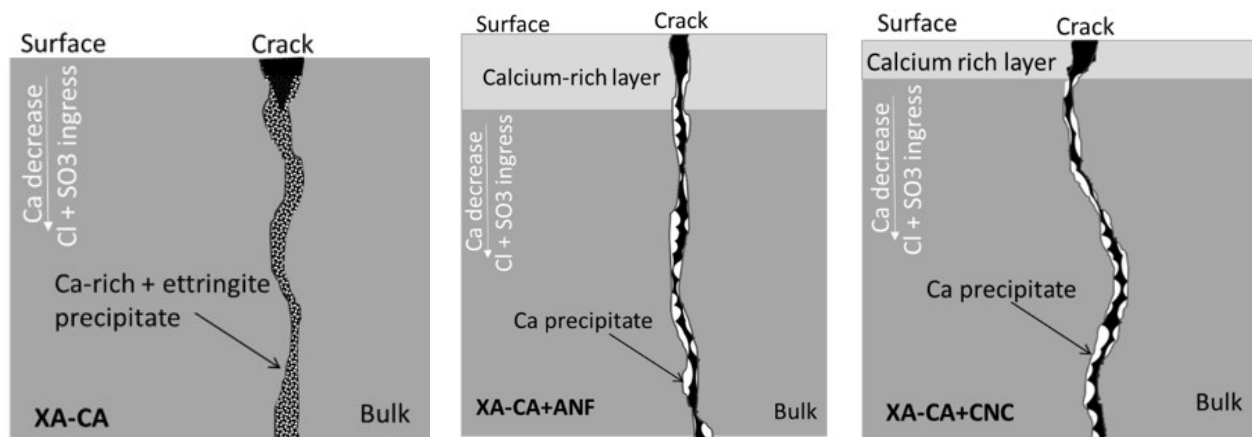


FIGURE 18. Scheme of the UHPFRC section after the dynamic test: concrete and crack.

According to the response of cracked UHPFRC in contact with waters rich in sulphate and chloride, a mechanism of interaction is proposed with regard to concrete composition and crack width: the simultaneous presence of several aggressive ions in the aggressive medium such as  $\text{Cl}^-$  and  $\text{SO}_4^{2-}$  suggest a combination of the action of both ions, the influence of sulphate being the most relevant for sgw and for the time under study. In addition, the waters cause the leaching and formation of a calcium-rich layer. Figure 18 shows a scheme of the composition and layers of the three UHPFRCs studied and the type and morphology of the precipitates formed in the crack, in agreement with the results of the dynamic sgw study, both in the crack and on the surface.

#### 4. CONCLUSIONS

The following conclusions are derived from the present study regarding the influence of aggressive media, the presence of cracks and UHPFRC nanoadditives:

- The electrical conductivity of the leaching medium is mainly affected by its initial ion content and the ions leached from the UHPFRCs studied due to chemical interactions. The presence of cracks produced no differences in response, nor did the incorporation of nanoadditives into the concrete composition.
- The effect of water movement and impact did not act as a self-damage promoter, but aggravated the damage caused by the aggressiveness of the medium.
- The convection regime and the chemical composition of the aggressive water affect the durability response of UHPFRC with BFS due to two chemical interaction processes: leaching and the formation of new phases and volume stability of the system in the aggressive media.

- The effect of water aggressiveness and temperature was recorded in the weight and length parameters but did not affect the evolution of the response.
- dw and sgw leachate alkalis and sgw provokes chloride and sulphate uptake as well as Na in order to balance the system.
- XA-CA+ANF and XA-CA+CNC showed a calcium-rich superficial layer, which was higher in the case of XA-CA+CNC. This layer acts as a protective layer and minimises the effect of sgw regarding ion interactions.
- After the test period, the UHPFRC showed partial precipitates but not the complete sealing of the cracks. Precipitate composition depends on crack width and the nanoadditive used: a calcite-rich layer in the case of XA-CA+ANF and XA-CA+CNC and ettringite in the case of CA-XA.

#### ACKNOWLEDGEMENTS

The research activity reported in this paper was performed in the framework of the ReSHEALience project, which has received funding from the European Union's Horizon 2020 research and innovation program under grant agreement No. 760824. The authors also thank L. Ferrara and E. Cuenca (Department of Civil and Environmental Engineering, Politecnico di Milano) for casting the different UHDC mixes investigated.

#### AUTHOR CONTRIBUTIONS:

Conceptualization: M.C. Alonso and E. Menéndez; Formal analysis: M.C. Alonso, E. Menéndez, M. Giménez, M. Criado; Funding acquisition: M.C. Alonso; Investigation: M. Giménez, M.C. Alonso; Methodology: M. Giménez, M.C. Alonso, E. Menéndez, M. Criado; Project administration: M.C. Alonso; Resources: EU-H2020; Roles/Writing, original draft: M. Giménez; Writing, review & editing: M. Giménez, M.C. Alonso, E. Menéndez, M. Criado.

## REFERENCES

- Van Damme, H. (2018) Concrete material science: Past, present, and future innovations. *Cem. Concr. Res.* 112, 5–24. <https://doi.org/10.1016/j.cemconres.2018.05.002>.
- Akhnoukh, A.K.; Buckhalter, C. (2021) Ultra-high-performance concrete: Constituents, mechanical properties, applications and current challenges. *Case Stud. Constr. Mat.* 15, e00559. <https://doi.org/10.1016/j.cscm.2021.e00559>.
- Reches, Y. (2018) Nanoparticles as concrete additives: Review and perspectives. *Constr. Build. Mat.* 175, 483–495. <https://doi.org/10.1016/j.conbuildmat.2018.04.214>.
- Shaikh, F.U.A.; Luhar, S.; Arel, H.S.; Luhar, I. (2020) Performance evaluation of Ultrahigh performance fibre reinforced concrete – A review. *Constr. Build. Mat.* 232, 117152. <https://doi.org/10.1016/j.conbuildmat.2019.117152>.
- Le Hoang, A.; Fehling, E. (2017) Influence of steel fiber content and aspect ratio on the uniaxial tensile and compressive behavior of ultra high performance concrete. *Constr. Build. Mat.* 153, 790–806. <https://doi.org/10.1016/j.conbuildmat.2017.07.130>.
- Fischer, G.; Li, V.C. (2007) Effect of fiber reinforcement on the response of structural members. *Eng. Fract. Mech.* 74 [1–2], 258–272. <https://doi.org/10.1016/j.engfracmech.2006.01.027>.
- Wang, W.; Liu, J.; Agostini, F.; Davy, C.A.; Skoczylas, F.; Corvez, D. (2014) Durability of an ultra high performance fibre reinforced concrete (UHPFRC) under progressive aging. *Cem. Concr. Res.* 55, 1–13. <https://doi.org/10.1016/j.cemconres.2013.09.008>.
- El-Joukhadar, N.; Pantazopoulou, S.J. (2021) Effectiveness of UHPFRC cover in delaying bar corrosion. *Constr. Build. Mat.* 269, 121288. <https://doi.org/10.1016/j.conbuildmat.2020.121288>.
- Prasanna, P.K.; Srinivasu, K.; Ramachandra Murthy, A. (2021) Strength and durability of fiber reinforced concrete with partial replacement of cement by Ground Granulated Blast Furnace Slag. *Mat. Today: Proceed.* ISSN 2214-7853.
- Luna, F.J.; Fernández, A.; Alonso, M.C. (2018) The influence of curing and aging on chloride transport through ternary blended cement concrete. *Mater. Construcc.* 68 [332], e171. <https://doi.org/10.3989/mc.2018.11917>.
- Higgins, D.D. (2003) Increased sulfate resistance of ggbs concrete in the presence of carbonate. *Cem. Concr. Comp.* 25 [8], 913–919. [https://doi.org/10.1016/S0958-9465\(03\)00148-3](https://doi.org/10.1016/S0958-9465(03)00148-3).
- Neville, A. (2004) The confused world of sulfate attack on concrete. *Cem. Concr. Res.* 34 [8], 1275–1296. <https://doi.org/10.1016/j.cemconres.2004.04.004>.
- Özbay, E.; Erdemir, M.; Durmuş, H.I. (2016) Utilization and efficiency of ground granulated blast furnace slag on concrete properties - A review. *Constr. Build. Mat.* 105, 423–434. <https://doi.org/10.1016/j.conbuildmat.2015.12.153>.
- Song, Q.; Yu, R.; Shui, Z.; Rao, S.; Fan, D.; Gao, X. (2020) Macro/micro characteristics variation of ultra-high performance fibre reinforced concrete (UHPFRC) subjected to critical marine environments. *Constr. Build. Mat.* 256, 119458. <https://doi.org/10.1016/j.conbuildmat.2020.119458>.
- Oh, B.H.; Jang, S.Y. (2007) Effects of material and environmental parameters on chloride penetration profiles in concrete structures. *Cem. Concr. Res.* 37 [1], 47–53. <https://doi.org/10.1016/j.cemconres.2006.09.005>.
- Yin, S.; Jing, L.; Yin, M.; Wang, B. (2019) Mechanical properties of textile reinforced concrete under chloride wet-dry and freeze-thaw cycle environments. *Cem. Concr. Comp.* 96, 118–127. <https://doi.org/10.1016/j.cemconcomp.2018.11.020>.
- Alonso, C.; Castellote, M.; Llorente, I.; Andrade, C. (2006) Ground water leaching resistance of high and ultra high performance concretes in relation to the testing convection regime. *Cem. Concr. Res.* 36 [9], 1583–1594. <https://doi.org/10.1016/j.cemconres.2006.04.004>.
- Wang, L.; He, T.; Zhou, Y.; Tang, S.; Tan, J.; Liu, Z.; Su, J. (2021) The influence of fiber type and length on the cracking resistance, durability and pore structure of face slab concrete. *Constr. Build. Mat.* 282, 122706. <https://doi.org/10.1016/j.conbuildmat.2021.122706>.
- Song, Q.; Yu, R.; Shui, Z.; Rao, S.; Wang, X.; Sun, M.; Jiang, C. (2018) Steel fibre content and interconnection induced electrochemical corrosion of ultra-high performance fibre reinforced concrete (UHPFRC). *Cem. Concr. Comp.* 94, 191–200. <https://doi.org/10.1016/j.cemconcomp.2018.09.010>.
- García Calvo, J.L.; Hidalgo, A.; Alonso, C.; Fernández Luco, L. (2010) Development of low-pH cementitious materials for HLRW repositories. Resistance against ground waters aggression. *Cem. Concr. Res.* 40 [8], 1290–1297. <https://doi.org/10.1016/j.cemconres.2009.11.008>.
- Qu, F.; Li, W.; Dong, W.; Tam, V. W. Y.; Yu, T. (2021) Durability deterioration of concrete under marine environment from material to structure: A critical review. *J. Build. Eng.* 35, 102074. <https://doi.org/10.1016/j.jobe.2020.102074>.
- Cheng, S.; Shui, Z.; Sun, T.; Gao, X.; Guo, C. (2019) Effects of sulfate and magnesium ion on the chloride transportation behavior and binding capacity of Portland cement mortar. *Constr. Build. Mat.* 204, 265–275. <https://doi.org/10.1016/j.conbuildmat.2019.01.132>.
- De Weerd, K.; Orsáková, D.; Geiker, M.R. (2014) The impact of sulphate and magnesium on chloride binding in Portland cement paste. *Cem. Concr. Res.* 65, 30–40. <https://doi.org/10.1016/j.cemconres.2014.07.007>.
- Menéndez, E. (2010) Análisis del hormigón en estructuras afectadas por reacción Arido-Alcali, ataque por sulfatos y ciclos Hielo-deshielo. Ed. IECA, España (2010).
- Alonso, M.C.; García Calvo, J.L.; Cuevas, J.; Turrero, M.J.; Fernández, R.; Torres, E.; Ruiz, A.I. (2017) Interaction processes at the concrete-bentonite interface after 13 years of FEBEX-Plug operation. Part I: Concrete alteration. *Phys. Chem. Earth.* 99, 38–48. <https://doi.org/10.1016/j.pce.2017.03.008>.
- Menéndez, E.; García-Rovés, R.; Aldea, B.; Ruíz, S.; Barrogel-Bouny, V. (2019) Combination of immersion and semi-immersion tests to evaluate concretes manufactured with sulfate-resisting cements. *J. Sust. Cem-Based Mat.* 8 [6], 337–352. <https://doi.org/10.1080/21650373.2019.1624659>.
- Pan, Z.; Zhu, Y.; Zhang, D.; Chen, N.; Yang, Y.; Cai, X. (2020) Effect of expansive agents on the workability, crack resistance and durability of shrinkage-compensating concrete with low contents of fibers. *Constr. Build. Mat.* 259, 119768. <https://doi.org/10.1016/j.conbuildmat.2020.119768>.
- Li, K.; Li, L. (2019) Crack-altered durability properties and performance of structural concretes. *Cem. Concr. Res.* 124, 105811. <https://doi.org/10.1016/j.cemconres.2019.105811>.
- Yousefieh, N.; Joushaghani, A.; Hajibandeh, E.; Shekarchi, M. (2017) Influence of fibers on drying shrinkage in restrained concrete. *Constr. Build. Mat.* 148, 833–845. <https://doi.org/10.1016/j.conbuildmat.2017.05.093>.
- Ren, J.; Lai, Y. (2021) Study on the durability and failure mechanism of concrete modified with nanoparticles and polypropylene fiber under freeze-thaw cycles and sulfate attack. *Cold. Reg. Sci. Tech.* 188, 103301. <https://doi.org/10.1016/j.coldregions.2021.103301>.
- Golewski, G. L. (2018) An assessment of microcracks in the Interfacial Transition Zone of durable concrete composites with fly ash additives. *Comp. Struct.* 200, 515–520. <https://doi.org/10.1016/j.compstruct.2018.05.144>.
- Ebrahimi, K.; Daiezadeh, M. J.; Zakertabrzi, M.; Zahmatkesh, F.; Habibnejad Korayem, A. (2018) A review of the impact of micro- and nanoparticles on freeze-thaw durability of hardened concrete: Mechanism perspective. *Constr. Build. Mat.* 186, 1105–1113. <https://doi.org/10.1016/j.conbuildmat.2018.08.029>.
- Roig-Flores, M.; Formagini, S.; Serna, P. (2021) Self-healing concrete-What Is it good for. *Mater. Construcc.* 71 [341], e237. <https://doi.org/10.3989/mc.2021.07320>.
- Singh, N.B.; Kalra, M.; Saxena, S.K. (2017) Nanoscience of Cement and Concrete. *Mat. Today: Proc.* 4 [4], 5478–5487. <https://doi.org/10.1016/j.matpr.2017.06.003>.
- Sanchez, F.; Sobolev, K. (2010) Nanotechnology in concrete - A review. *Constr. Build. Mat.* 24 [11], 2060–2071. <https://doi.org/10.1016/j.conbuildmat.2010.03.014>.
- Sobolev, K. (2016) Modern developments related to nanotechnology and nanoengineering of concrete. *Front. Struct. Civ. Eng.* 10, 131–141. <https://doi.org/10.1007/s11709-016-0343-0>.
- Gopalakrishnan, R.; Jeyalakshmi, R. (2018) Strength deterioration of nano-silica contained in ordinary Portland cement concretes in aggressive sulfate environments. *Eur. Phys. J. Plus.* 133, 351. <https://doi.org/10.1140/epjp/i2018-12162-3>.
- Ferrara, L.; Krelani, V.; Carsana, M. (2014) A “fracture testing” based approach to assess crack healing of concrete with

- and without crystalline admixtures. *Constr. Build. Mat.* 68, 535–551. <https://doi.org/10.1016/j.conbuildmat.2014.07.008>.
39. Nasim, M.; Dewangan, U.K.; Deo, S.V. (2020) Autonomous healing in concrete by crystalline admixture: A review. *Mat. Today: Procc.* 32, 638–644. <https://doi.org/10.1016/j.matpr.2020.03.116>.
  40. Sisomphon, K.; Copuroglu, O.; Koenders, E.A.B. (2012) Self-healing of surface cracks in mortars with expansive additive and crystalline additive. *Cem. Concr. Comp.* 34 [4], 566–574. <https://doi.org/10.1016/j.cemconcomp.2012.01.005>.
  41. Li, Z.; Wang, H.; He, S.; Lu, Y.; Wang, M. (2006) Investigations on the preparation and mechanical properties of the nano-alumina reinforced cement composite. *Mat. Letters.* 60 [3], 356–359. <https://doi.org/10.1016/j.matlet.2005.08.061>.
  42. Cao, Y.; Zavaterra, P.; Youngblood, J.; Moon, R.; Weiss, J. (2015) The influence of cellulose nanocrystal additions on the performance of cement paste. *Cem. Concr. Comp.* 56, 73–83. <https://doi.org/10.1016/j.cemconcomp.2014.11.008>.
  43. Behfarnia, K.; Salemi, N. (2013) The effects of nano-silica and nano-alumina on frost resistance of normal concrete. *Constr. Build. Mat.* 48, 580–584. <https://doi.org/10.1016/j.conbuildmat.2013.07.088>.
  44. Lee, S.J.; Kawashima, S.; Kim, K.J.; Woo, S.K.; Won, J.P. (2018) Shrinkage characteristics and strength recovery of nanomaterials-cement composites. *Comp. Struct.* 202, 559–565. <https://doi.org/10.1016/j.compstruct.2018.03.003>.
  45. Kawashima, S.; Shah, S.P. (2011) Early-age autogenous and drying shrinkage behavior of cellulose fiber-reinforced cementitious materials. *Cem. Concr. Comp.* 33 [2], 201–208. <https://doi.org/10.1016/j.cemconcomp.2010.10.018>.
  46. Cuenca, E.; Mezzena, A.; Ferrara, L. (2021) Synergy between crystalline admixtures and nano-constituents in enhancing autogenous healing capacity of cementitious composites under cracking and healing cycles in aggressive waters. *Constr. Build. Mat.* 266, Part B, 121447. <https://doi.org/10.1016/j.conbuildmat.2020.121447>.
  47. Cuenca, E.; Criado, M.; Giménez, M.; Alonso, M.C. (2021) Effects of alumina nanofibers and cellulose nanocrystals on durability and self-healing capacity of ultra-high performance fiber reinforced concretes (UHPRFC). *J. Mater.*, *accepted*.
  48. Kumar, S.; Kumar, R.; Bandopadhyay, A.; Alex, T.C.; Ravi Kumar, B.; Das, S.K.; Mehrotra, S.P. (2008) Mechanical activation of granulated blast furnace slag and its effect on the properties and structure of portland slag cement. *Cem. Concr. Comp.* 30 [8], 679–685. <https://doi.org/10.1016/j.cemconcomp.2008.05.005>.
  49. Zuquan, J.; Wei, S.; Yunsheng, Z.; Jinyang, J.; Jianzhong, L. (2007) Interaction between sulfate and chloride solution attack of concretes with and without fly ash. *Cem. Concr. Res.* 37 [8], 1223–1232. <https://doi.org/10.1016/j.cemconres.2007.02.016>.
  50. Guo, J.J.; Wang, K.; Guo, T.; Yang, Z.Y.; Zhang, P. (2019) Effect of dry-wet ratio on properties of concrete under sulfate attack. *Mater.* 12 [7], 2755. <https://doi.org/10.3390/ma12172755>.
  51. García Calvo, J.L.; Alonso, M.C.; Hidalgo, A.; Fernández Luco, L.; Flor-Laguna, V. (2013) Development of low-pH cementitious materials based on CAC for HLW repositories: Long-term hydration and resistance against ground-water aggression. *Cem. Concr. Res.* 51, 67–77. <https://doi.org/10.1016/j.cemconres.2013.04.008>.
  52. Santillán, L.R.; Locati, F.; Villagrán-Zaccardi, Y.A.; Zega, C.J. (2020) Long-term sulfate attack on recycled aggregate concrete immersed in sodium sulfate solution for 10 years. *Mater. Construcc.* 70 [337], e212. <https://doi.org/10.3989/mc.2020.06319>.
  53. Taylor, H.F. W.; Famy, C.; Scrivener, K.L. (2001) Delayed ettringite formation. *Cem. Concr. Res.* 31 [5], 683–693. [https://doi.org/10.1016/S0008-8846\(01\)00466-5](https://doi.org/10.1016/S0008-8846(01)00466-5).